

# Some Fundamental Aspects about Lipschitz Continuity of Neural Networks

Grigory Khromov\*<sup>a</sup> and Sidak Pal Singh\*<sup>a,b</sup>

<sup>a</sup> Department of Computer Science, ETH Zürich

<sup>b</sup> Max Planck ETH Center for Learning Systems

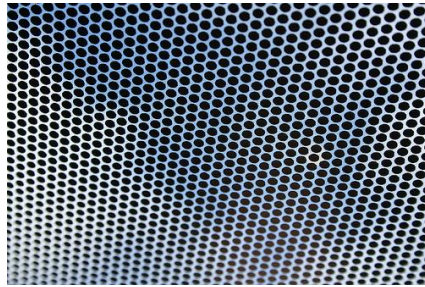
## Abstract

Lipschitz continuity is a simple yet crucial functional property of any predictive model for it lies at the core of the model’s robustness, generalisation, as well as adversarial vulnerability. Our aim is to thoroughly investigate and characterise the Lipschitz behaviour of the functions realised by neural networks. Thus, we carry out an empirical investigation in a range of different settings (namely, architectures, losses, optimisers, label noise, and more) by exhausting the limits of the simplest and the most general lower and upper bounds. Although motivated primarily by computational hardness results, this choice nevertheless turns out to be rather resourceful and sheds light on several fundamental and intriguing traits of the Lipschitz continuity of neural network functions, which we also supplement with suitable theoretical arguments. As a highlight of this investigation, we identify *a striking double descent trend in both upper and lower bounds to the Lipschitz constant* with increasing network width — which tightly aligns with the typical double descent trend in the test loss. Lastly, we touch upon the seeming (counter-intuitive) decline of the Lipschitz constant in the presence of label noise.

## 1 Introduction



(a) ImageNet sample with the **highest** Jacobian norm of 278.65 (the label is ‘park bench’).



(b) ImageNet sample with the **smallest** Jacobian norm of 3.11 (the label is ‘window screen’).

Figure 1: The most and least sensitive images for an ImageNet-trained ResNet18 network, as measured via per-sample Jacobian norms. So, the lower bound to its Lipschitz constant is  $\geq 278.65$ .

Lipschitz continuity of a function is a key property that reflects its smoothness as the input is perturbed (more accurately, the maximum absolute change in the function value per unit norm change in the

\*Equal Contribution. Correspondence to [gkhromov@ethz.ch](mailto:gkhromov@ethz.ch), [ssidak@ethz.ch](mailto:ssidak@ethz.ch).

input). Typically, in machine learning, we desire that the learned predictive function is robust, i.e., not overly sensitive to changes in the input. If achieving pointwise robustness in the entire input space is difficult, then we would hope to be robust over as large and representative a subset of the input space with respect to the underlying data distribution (like in the vicinity of the training samples). For instance, Figure 1 indicates two exemplar training samples, where the sensitivity of the function (learnt by ResNet18) to local input perturbations is the highest and the lowest respectively. So, on one hand, if the function changes too drastically in response to minuscule changes in the input, especially if the input is near the decision boundary or from another representative region, we can hardly be confident that the learned function generalises on unseen test data. But, on the flip side, when the value of the Lipschitz constant associated with the corresponding Lipschitz continuity is extremely small (for the sake of the argument, think zero) over the entire input space, this would imply an excessively large bias [1] and essentially a useless function.

Hence, it should be evident why the Lipschitz constant plays such a crucial role in various topics such as generalisation [2], robustness [3], vulnerability to adversarial examples [4, 5], and more. As a result, there is also a significant body of literature in both theoretical [2, 6–10] and applied [11–15] directions, as discussed below in more detail.

**Aim of our study.** In contrast, we would like to focus more on exploring and uncovering fundamental aspects of Lipschitz continuity of neural network functions — and thus contribute towards a better understanding of modern over-parameterised neural networks. This is because despite much progress achieved over the years — owing to which we have better estimates of the true Lipschitz constant [6] — insights about the behaviour and characteristics of Lipschitz continuity for neural networks have been hard to come by. More precisely, several fundamental questions in this context remain to be adequately addressed, such as:

- How does the Lipschitz constant behave across wide and narrow networks, or say across shallow and deep networks?
- Does the Lipschitz constant change significantly over the course of training or is it largely governed by the value at initialisation?
- How does its behaviour vary across different loss functions? (Since, if we want to arrive at ‘functional’ properties, we don’t want to be misled by the choice of a particular loss function.)
- How does the nature of the learning task (i.e., in terms of the amount of signal or noise present in features and labels) affect the Lipschitz continuity?

Our objective is to contribute towards this end, with an emphasis on finite-width over-parameterised deep neural networks as trained in practice.

**Approach.** Part of the reason why important insights have been hard to come by through recent studies on the Lipschitz constant is that the newer methods, which produce tighter estimates of the true Lipschitz are, more often than not, rather computationally expensive which greatly limits their use. Or when simple bounds are utilised, there is an element of uncertainty whether the findings apply to the true Lipschitz constant or just that particular bound.

However, in this paper, we propose to sidestep this issue by first trying to exhaust or reach the limits of the insights that can be extracted via the simplest bounds. Concretely, we track and investigate both upper and lower bounds to the Lipschitz constant, thereby ‘sandwiching’ the true value in between. This embarrassingly simple shift in research perspective lets us demonstrate intriguing traits about the Lipschitz constant of neural network functions in a multitude of settings.

**Contributions.** (i) To begin with, in Section 4.1, we investigate the evolution of upper and lower bounds to the Lipschitz constant during the course of training for fully-connected and convolutional networks. Here, we also showcase the fidelity of the lower bounds to represent the true Lipschitz constant by evaluating them in a much wider vicinity of the training samples. (ii) We validate our findings about the fidelity of the lower Lipschitz on the unparalleled setting of ResNet50 on ImageNet. (iii) We then study the effect of increasing network widths on the Lipschitz constant, within an extensive range of widths spanning about 14 orders of magnitude, connecting our findings with the Double Descent phenomenon [16]. We complement this empirical finding by sketching a theoretical argument for this behaviour using the bias-variance tradeoff. (iv) Finally, we proceed with an investigation of the behaviour of the Lipschitz constant in the presence of label noise. Besides,

in the main text, we also briefly allude to the effects of different loss functions, optimisers, training set size, and more, on the behaviour of Lipschitz continuity and offer potential reasons for the same. Lastly, we find that the distance of the network from the initialisation can capture many of the interesting trends in the Lipschitz constant.

## 2 Related Work

Theoretical interest in the Lipschitz constant of neural networks has been revived since Bartlett et al. [2] described how margin-based generalisation bounds are linearly dependent on the Lipschitz constant. Since generalisation bounds and robustness guarantees [3] are expressed in terms of the upper bound estimates of the true Lipschitz constant, extensive research has been done in the field of its efficient and accurate estimation [6, 7, 9, 10, 17]. Bubeck and Sellke [18] have also tied the phenomena of smooth interpolation in overparametrised networks with the underlying Lipschitz continuity of the network.

On the practical side, Lipschitz constant has also been useful to provide stability [19] and robustness guarantees for regular neural networks [11, 12, 20] by enforcing certain Lipschitz continuity in its intermediate layers (for instance, one can achieve that by modification of the layer [21]). Similar techniques were also studied for Convolutional networks [13], Generative Adversarial Networks (GANs) [14, 22], Equilibrium Networks [23] and Reinforcement Learning settings [24]. By its definition, Lipschitz constant is tightly related to quantifying the effects of input perturbation and is therefore pervasive in relevant papers [15]. Alternatively, one can also modify the training procedure to enforce certain Lipschitz continuity to certify the robustness of networks [25–28], stabilise GAN training [29–31] and improve adversarial vulnerability [32].

Concurrent with the release of our work, Gamba et al. [33] have also noted the connection between Lipschitz constant and the phenomenon of double descent [34], albeit by tracking only a reasonable estimate of the Lipschitz and not both the lower and upper Lipschitz bounds as considered here. But most importantly, our focus is also much more comprehensive (i.e., not just double descent) as we explore the fidelity of the lower bound in detail and discuss many other settings to elucidate the behaviour of Lipschitz constant.

## 3 Preliminaries and Setup

### 3.1 Theoretical Preliminaries

Before we start investigating the Lipschitz constant for neural networks, let us first recall the definition of Lipschitz-continuous functions.

**Definition 3.1 (Lipschitz continuous function)** For function  $f : \mathbb{R}^d \mapsto \mathbb{R}^K$ , defined on some domain  $\text{dom}(f) \subseteq \mathbb{R}^d$ ,  $f$  is called  $C$ -Lipschitz continuous,  $C > 0$ , w.r.t some  $\alpha$ -norm if:

$$\forall \mathbf{x}, \mathbf{y} \in \text{dom}(f) : \|f(\mathbf{x}) - f(\mathbf{y})\|_\alpha \leq C \|\mathbf{x} - \mathbf{y}\|_\alpha.$$

Note that we are usually interested in the smallest  $C$ , such that the above condition holds. This is what we call the Lipschitz constant of the function  $f$ . Unfortunately, the exact value of the Lipschitz constant has been proven to be NP-hard to compute [17]. Therefore, we focus on the upper and lower bounding the true Lipschitz constant. To lower bound the Lipschitz constant, we will need an alternative definition of the Lipschitz constant,

**Lemma 3.1 (Alternative definition [10, 35])** Let function  $f : \mathbb{R}^d \mapsto \mathbb{R}^K$ , be defined on some domain  $\text{dom}(f) \subseteq \mathbb{R}^d$ . Let  $f$  also be differentiable and  $C$ -Lipschitz continuous. Then the Lipschitz constant  $C$  is given by:

$$C = \sup_{\mathbf{x} \in \text{dom}(f)} \|\nabla_{\mathbf{x}} f\|_{\alpha^*},$$

where  $\nabla_{\mathbf{x}} f$  is the Jacobian of  $f$  w.r.t. to input  $\mathbf{x}$  and  $\alpha^*$  is the dual norm of  $\alpha$ .

For simplicity, we will focus on computing the 2-norm for the rest of the paper. Note that the dual norm for the 2-norm is also 2-norm. Hereafter, all the norms will denote the 2-norm, and thus we will omit it in the expressions.

**Lower bound via local Lipschitz continuity.** Instead of considering the global Lipschitz constant, i.e., over the entire input domain  $\text{dom}(f)$ , we can restrict ourselves to the subspace of the domain where the underlying data distribution  $\mathcal{D}$  is supported, and its neighbourhood. Under the *i.i.d.* (independent and identically distributed) assumption in which we typically operate, this local Lipschitz continuity (and the associated constant  $C_{\text{local}}$ ) carries a direct significance. Moreover, this also provides a natural way to lower bound the local Lipschitz constant (which itself lower bounds the global Lipschitz  $C$ ) based on a finite-sample evaluation, like on the training set  $S \subseteq \mathcal{D}$ :

$$C \geq C_{\text{local}} = \sup_{\mathbf{x} \in \mathcal{D}} \|\nabla_{\mathbf{x}} f_{\boldsymbol{\theta}}\|_2 \geq \sup_{\mathbf{x} \in S} \|\nabla_{\mathbf{x}} f_{\boldsymbol{\theta}}\|_2 =: C_{\text{lower}} \quad (1)$$

**Upper bound via product of layerwise upper bounds.** Tight upper bounds to the Lipschitz constant, however, are far from straightforward to compute, as discussed at length in Section 2. As mentioned before, our aim in this paper is not to come up with or probe the tightest upper bounds, but rather extract the most out of the simplest bounds. So, as expected, we upper bound the Lipschitz constant of the network by multiplying per-layer upper bounds. Let us assume we have a network  $f_{\boldsymbol{\theta}}$  with  $L$  layers, 1-Lipschitz non-linearity or activation function  $\sigma$ , such as ReLU, and parameters  $\boldsymbol{\theta} \in \mathbb{R}^p$ . The overall function can be then expressed as  $f_{\boldsymbol{\theta}} := f^{(L)} \circ \sigma \circ f^{(L-1)} \circ \sigma \circ \dots \circ f^{(1)}$ ,

$$C \leq \prod_{i=1}^L \sup_{\mathbf{x}^{(i-1)} \in \text{dom}(f^{(i)})} \|\nabla_{\mathbf{x}^{(i-1)}} f^{(i)}\| \leq \prod_{i=1}^L \sup \|\nabla_{\mathbf{x}^{(i-1)}} f^{(i)}\| =: C_{\text{upper}} \quad (2)$$

where  $\mathbf{x}^{(i-1)}$  denotes the input at the layer  $i$ , i.e., the post-activation at layer  $i - 1$ . In the above equation, we just used 1-Lipschitzness of the non-linearity and then considered an unconstrained supremum. As a simple example, take the case of a single linear layer  $f^{(1)}(\mathbf{x}) = \mathbf{W}^{(1)} \mathbf{x}$ , and so the upper bound to the Lipschitz constant is clearly equal to the spectral norm of the weight matrix, i.e.,  $C_{\text{upper}} = \|\mathbf{W}^{(1)}\|_2$ . Similarly, for an  $L$ -layer network, the upper bound just equals the product of the spectral norms of the weight matrices,  $C_{\text{upper}} = \prod_{i=1}^L \|\mathbf{W}^{(i)}\|_2$ . More details on this, such as how this extends to the case of other networks can be found in Appendix S1.1.

### 3.2 Empirical Setup

We benchmark our findings in a wide variety of settings, with different choices of (a) *architectures*: fully-connected networks (FCNs), convolutional neural networks (CNNs), Residual networks (ResNets); (b) *datasets*: CIFAR10, MNIST, MNIST1D [36] (a harder version of usual MNIST), as well as ImageNet; (c) *loss functions*: Mean-Squared Error (MSE) and Cross-Entropy (CE) loss. While we only present the representative results for the experiments in the upcoming sections, the comprehensive results across all the settings along with experimental details can be found in the Appendices S1 and S2. Unless stated otherwise, the results in the main paper are based on stochastic gradient descent with CE loss. All the presented results have been averaged over 4 runs.

## 4 Insights into the nature of the Lipschitz constant

### 4.1 How does the Lipschitz constant evolve and what is it really like?

*Evolution of the Lipschitz constant.* Let us begin by first exploring how the Lipschitz constant evolves during training. In Figure 2, we present the results of training a fully-connected network (FCN) with ReLU activations (or, FCN ReLU as shorthand) until convergence. We observe that both the  $C_{\text{lower}}$  and the  $C_{\text{upper}}$  keep increasing as the training proceeds. While they start from similar values at initialization, they rapidly diverge from each other. Moreover, we find that the trend of the Lipschitz bounds stabilizes after some time into training, beyond which they grow at a linear rate (in log scale).

To ensure that the trend of the lower Lipschitz is representative of the dataset at large, and does not just arise from the presence of some outliers, we additionally plot  $C_{\text{avg\_norm}} = \mathbb{E}_{\mathbf{x} \in S} \|\nabla_{\mathbf{x}} f_{\boldsymbol{\theta}}\|_2$ , i.e., the expected value of the Jacobian norm. It turns out that the trend of this  $C_{\text{avg\_norm}}$  is indeed rather similar to  $C_{\text{lower}}$ , and the latter is representative of the overall dataset. Besides, the above *Lipschitz evolution trends hold consistently for other datasets such as CIFAR-10 and MNIST*; with MSE loss; as well as when CNNs are used in place of FCNs (see S2.2).

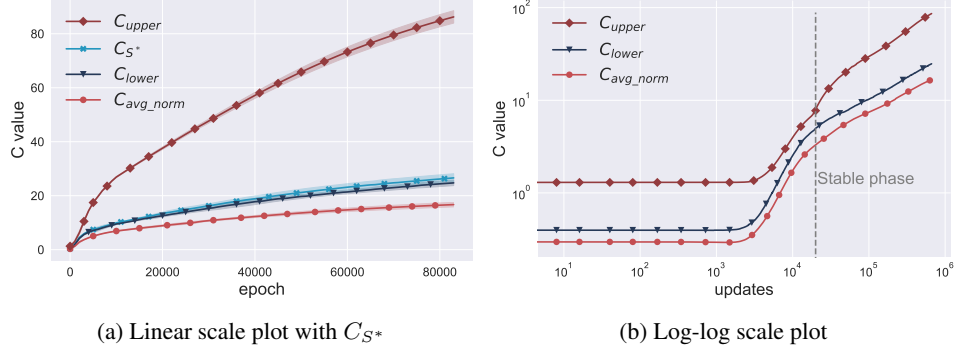


Figure 2: Plot of Lipschitz constant bounds by training epoch for **FCN ReLU network** with 1 hidden layer with 256 neurons trained on MNIST1D.  $C_{upper}$ ,  $C_{lower}$  and  $C_{avg\_norm}$  are computed on train dataset  $S$ , whereas  $C_{S^*}$  is the local Lipschitz computed on the  $S^*$ . In the stable phase, the slopes for the upper, lower, and average Lipschitz bounds are: 0.59, 0.46, 0.44 respectively. Results are averaged over 4 runs. More details in Appendix S1.5.5.

*Fidelity of the lower bound to the true Lipschitz.* As the true Lipschitz constant lies somewhere between the upper and the lower bounds, it is quite natural to enquire how loose are those bounds and where our quantity of interest lies. To give more insight into this, we compute the lower bound in Eqn.1 on a larger set of examples  $S^*$ , which is the union of the training set  $S$ , the test set  $S'$ , and a set of random convex combinations of samples from the train and test sets (see S1.5.5 for more details). The results are presented in Figure 2a, corresponding to the legend  $C_{S^*}$ , where it becomes evident that the bound for the Lipschitz constant computed on this expanded set  $S^*$  lies closer to the lower bound  $C_{lower}$  than the upper bound. While the gap between the upper and the lower bound may not seem that drastic here, the upper bound can quickly become extremely large for deeper models (c.f., fig. 3 and appendix S2.2), leading to a significant overestimation of the Lipschitz constant of the network function. In fact, this aspect can also be spotted in some of the works [10] which propose tight upper bounds to the Lipschitz constant. Overall, this suggests that *the trend of true Lipschitz constant is more faithfully captured by the lower bound  $C_{lower}$  instead of the upper bound  $C_{upper}$* .

*Other Remarks.* As can be seen, we have evaluated the fidelity of our lower bound on samples in the input space that are outside of the data distribution (but are still somewhat meaningful). It would also be interesting to consider the case of adversarially generated samples [4] and see how much can the lower bounds be pushed up, but we leave this for a future investigation.

**A theoretical picture.** To understand this analytically, we relate the variation in the function  $f(\theta^T, \cdot)$  values at inputs  $\mathbf{x}, \mathbf{x}'$  after training for  $T$  steps to the corresponding total distance travelled in the parameter space and the Lipschitz constant at initialization. With a suitable telescoping analysis of the function variation at the intermediate steps in training, as detailed in Appendix S3.1, we obtain:

$$\|f(\theta^T, \mathbf{x}) - f(\theta^T, \mathbf{x}')\| \leq \left( \frac{2}{r} C_{\theta}^{\text{local}} \sum_{t=0}^{T-1} \|\theta^{t+1} - \theta^t\| + C_{\mathbf{x}}(\theta^0) \right) r, \quad (3)$$

where  $r = \sup_{\mathbf{x}, \mathbf{x}' \in \mathcal{D}} \|\mathbf{x} - \mathbf{x}'\|$  denotes the diameter of the input space,  $C_{\mathbf{x}}(\theta^0)$  is the Lipschitz constant in the input space for the model at initialisation, and  $C_{\theta}^{\text{local}}$  is a measure of the local Lipschitz constant in the parameter space. For simplicity, if we consider the SGD update rule during training, along with a constant learning rate  $\eta \in (0, \infty)$  and assume the loss gradients are bounded above by  $B \in (0, \infty)$  (which could be enforced by gradient clipping, for instance) we get that true Lipschitz constant,  $C_T$  for the function at the  $T$ -th step is lower bounded as,  $C_T \geq \frac{2}{r} C_{\theta}^{\text{local}} B \eta T + C_{\mathbf{x}}(\theta^0)$ .

Moreover, under our assumptions of constant learning rate, we also get  $C_T \propto T$ . In other words, this suggests the Lipschitz constant grows linearly with the number of training steps, which qualitatively aligns with the observations from our evolution experiments. There is a lot of room for improvement in the above analysis, some of which we also discuss in Appendix S3.1, but this already reveals interesting dependencies of the Lipschitz constant.



## 4.2 What happens for bigger network-dataset settings?

Our primary aim in this work is to uncover the key characteristics of the Lipschitz constant, and not necessarily to attain the best-performing networks. Hence, in the previous section, we focused on small networks that elucidate the point while still being as accurate in our empirical Lipschitz estimates (e.g., estimating it over the entire dataset throughout training), within the constraints of our limited resources. However, to establish that our results do indeed scale for over-parameterized networks with millions of parameters, we take the case of ResNet50 trained on ImageNet and study the evolution of Lipschitz over 10 checkpoints in training and multiple seeds, as an exemplar setting.

So, in this case, computing the lower Lipschitz would require computing  $\sim 1.2$  million Jacobian matrices of size  $1,000 \times 1,50,528$ , for a single seed and a single checkpoint. As a reference point, training a ResNet50 for 90 epochs with a batch size of 1024 on ImageNet requires  $\sim 1,06,000$  gradient evaluations. Hence, each lower Lipschitz estimation is almost as expensive as one entire training run. To ease the computational burden, we evaluate the lower Lipschitz on a 200,000 sized subset of the training set (the potential error introduced due to this subsampling procedure is minimal, as shown in Appendix S2.1).

Likewise, computing the upper bound is not a cakewalk either. We need to compute the spectral norms of the equivalent matrix representation of the convolutional kernels, which can be rather large in size if represented naively and we have to resort to sparse matrix representations. Having understood the scale of the challenge, let us take a look at the evolution plots in Figure 3. We find that they essentially follow a trend similar to what was previously shown for fully connected networks (Figure 2). However, taking a closer look, we find that the upper bound gets almost vacuously large, being 38 orders of magnitude larger than the lower bound. The slopes of the log-log slope after epoch 60 for the upper, lower, and average Lipschitz bounds are 7.324, 0.494, 0.475 respectively.

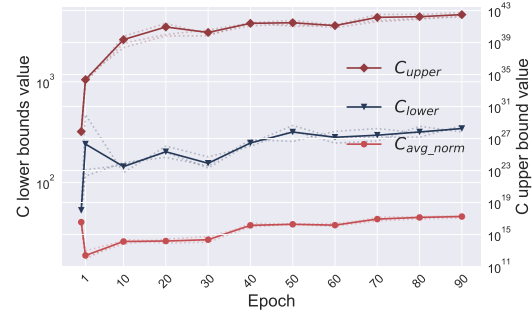


Figure 3: Plot of Lipschitz constant bounds by training epoch for ResNet50 on a subset of 200,000 samples of ImageNet. Results are averaged over 3 runs. More details in Appendix S1.5.6.

This suggests that upper bounds are excessively lax (even at initialization itself, it is of the order  $1e^{27}$ , which can be attributed to the exponential increase with depth) and barely tell us anything about the true Lipschitz or the nature of the function in general, while lower bounds are more representative.

**Fidelity of the lower bound to the true Lipschitz, once more.** Given the extremely high values of the upper bound, it can be debated whether our computed lower bounds still representative of the true Lipschitz. To counter this, we take the top 1,000 samples that have the highest Jacobian norm, consider their convex combinations, and use that as a basis to evaluate the lower Lipschitz bounds. In fact, in Figure 4, we show the entire distribution of norms for these ‘hard’ convex combinations as well as the entire ImageNet training set.

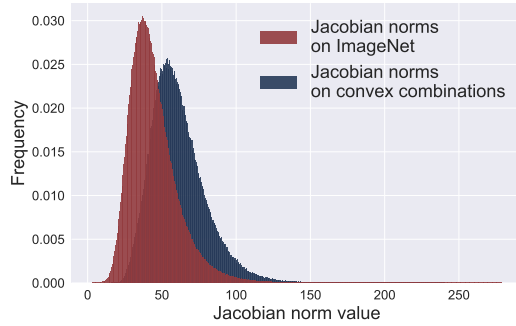


Figure 4: Distribution of the norm of the per-sample Jacobian for pretrained ResNet18, computed on the entire ImageNet and 1,000,000 hard convex combinations on ImageNet (See Appendix S1.5.7 for more).

We find that while the distribution indeed shifts towards larger per-sample Jacobian norms for the hard convex combinations, the shift is not even a multiplicative factor of  $2\times$  more. This shift pales in comparison to the upper bound which is over tens of orders of magnitudes higher. Overall, this strengthens our claim that the lower bound is much more faithful to the true Lipschitz value and can hence serve better

to explore various phenomenon observed in over-parameterized neural networks. Lastly, similar distribution plots for other models and datasets in Appendix S2.10.

### 4.3 The phenomenon of Lipschitz Double Descent with Width

To study how the Lipschitz constant changes with the width of the hidden layers of the model, we conduct an experiment where we trained 16 FCN-ReLU networks, with 1 hidden layer, of increasing widths from 16 to 131, 072. This arrangement should be reminiscent of the Double Descent setup [34], which we indeed replicated for our setting. More details on models and the training strategy are listed in Appendix S1. Figure 5 clearly displays how all three Lipschitz constant bounds display a shape similar to Double Descent, growing until the interpolation threshold (where the number of parameters  $p$  approximately equals the number of samples  $n$ ) and then decreasing afterwards.

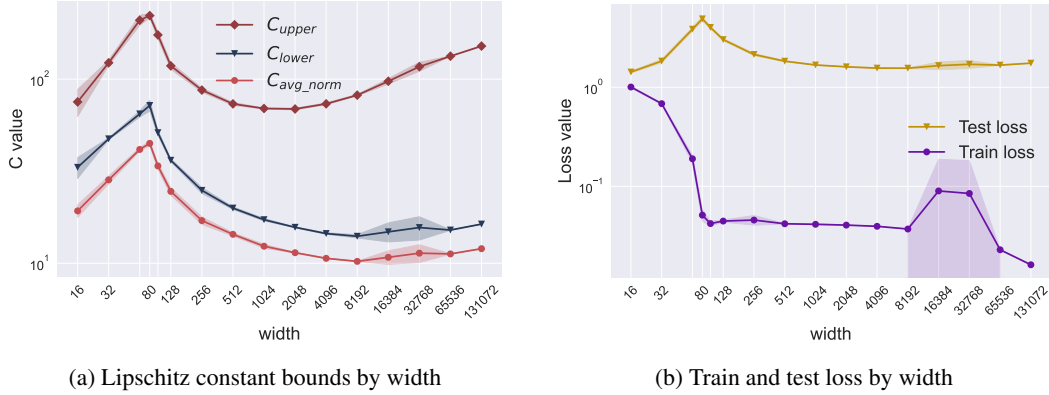


Figure 5: Comparison of various Lipschitz constant bounds with train and test losses with increasing hidden layer width, in the case of **FCN ReLU networks** on **MNIST1D**. Results are averaged over 4 runs. More details about the networks and the training strategy are listed in Appendix S1.5.1.

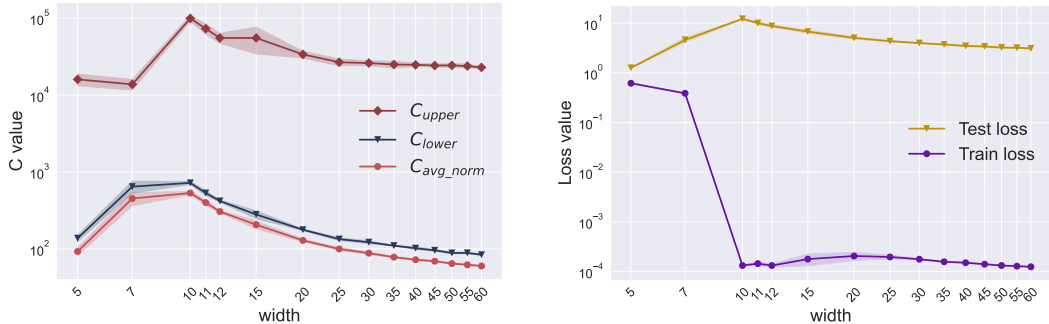


Figure 6: Comparison of various Lipschitz constant bounds with train and test losses with increasing hidden layer width, in the case of **CNN networks** on **CIFAR-10**. Results are averaged over 4 runs. More details about the networks and the training strategy are listed in Appendix S1.5.3.

Similar trends in the Lipschitz constant can also be seen for fully-connected ReLU networks trained using MSE loss, as well as CNNs trained on CIFAR-10 and MNIST S2.3 using Cross-Entropy. We also include additional experiments on top of previously observed double descent in test loss in the literature [37], where we simply plot the Lipschitz bounds and, remarkably, we even observe a double descent trend for them S2.4.

*Remarks.* (a) *Generalization bounds:* The fact that Lipschitz constant shows the same trend as the test loss is in a way expected, given that several generalization bounds include it as a term [2]. It would also be interesting to investigate if such proposed bounds also capture double descent in their entirety, and not just when the trend of the Lipschitz constant is noted in isolation. (b) *Triple Descent:* Like the test loss, the upper Lipschitz for FCN ReLU networks seems to continue to increase after

the second descent, which could potentially be tied to the Triple Descent phenomenon [38], where the test loss shows another peak for  $p \approx n^2$ . We leave this interesting observation for future research.

**A textbook bias-variance tradeoff argument.** In this section, we provide a brief theoretical analysis to connect Lipschitz behaviour with the test loss. Let us denote the neural network function as  $f_{\theta}(\mathbf{x}, \zeta)$ . Here,  $\zeta$  indicates the noise in the function due to the choice of random initialisation and that introduced by a stochastic optimiser, like SGD. By considering the fixed-design variant of the bias-variance tradeoff (i.e., we will not average over the choice of the training set sampled from the distribution), we can write the expected test MSE loss  $\mathcal{L}(\theta, S', \zeta)$  on the test dataset  $S'$  as a sum of squared bias and variance:

$$\mathbb{E}_{\zeta} [\mathcal{L}(\theta, S', \zeta)] = \mathbb{E}_{\mathbf{x} \sim S'} [\|y(\mathbf{x}) - \mathbb{E}_{\zeta}[f_{\theta}(\mathbf{x}, \zeta)]\|^2] + \mathbb{E}_{\mathbf{x} \sim S'} [\text{Var}_{\zeta}(f_{\theta}(\mathbf{x}, \zeta))] .$$

One can show that the variance term can be upper bounded by a constant plus a quantity that is proportional to the sum of the squares of the mean Lipschitz constant across seeds  $\overline{C}_{\zeta}$  and the Lipschitz constant  $\overline{C}$  of the ensembled function  $\overline{f}_{\theta}(\cdot) = \mathbb{E}_{\zeta}[f_{\theta}(\cdot, \zeta)]$ . More details are listed in Appendix S3.2.

$$\mathbb{E}_{\mathbf{x} \sim S'} \text{Var}_{\zeta}(f_{\theta}(\mathbf{x}, \zeta)) \leq 3(\overline{C}^2 + \overline{C}_{\zeta}^2) \mathbb{E}_{\mathbf{x} \sim S'} \|\mathbf{x}\|^2 + \text{constant} \quad (\text{Var bound 1})$$

In Figure 7, we present an empirical calculation for the bias-variance analysis, where the trend of the function variance aligns closely with the trend of our upper bounds, at least qualitatively. Since the above theoretical analysis only establishes an upper bound on the function variance with the Lipschitz constant, it would be very interesting to develop a corresponding lower bound that shows the dependence on the Lipschitz constant. But that is beyond the scope of our current work.

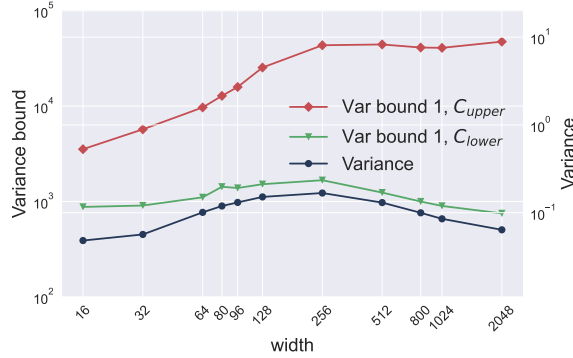


Figure 7: Variance and its upper bounds, where  $\overline{C}_{\zeta}$  in **Var bound 1** is estimated using  $C_{lower}$  and  $C_{upper}$  estimates. Results are presented from training FCN LeakyReLU networks with varying width on MNIST1D using MSE loss. The expectations over random initialisations were computed as an average of 4 seeds. More details in Appendix S1.5.8.

#### 4.4 Label noise

It has been emphatically shown [39], that while over-parameterized neural networks have the ability to completely memorize points with random labels, they do not memorize nominally (i.e., in the absence of such noise) and continue to generalize. As the Lipschitz constant is a natural indicator of the smoothness of the learnt function, we explore if captures the trend of the worsening generalisation with increasing label noise.

We carry out this analysis for several 5-hidden layer CNNs trained on CIFAR10. The results for two such networks, namely CNN10 and CNN20, are located in Figure 8a. In the case of CNN10, as expected, the lower Lipschitz increases with increasing label noise. However, in the case of the wider CNN20, we see a surprising behaviour: the lower Lipschitz stalls and then somewhat decreases with more label noise. To understand this better, in Figure 8b, we inspect how the distance from the initialization behaves, where interestingly, similar trends also show up.

Our experiments suggest that label noise may have a more subtle effect in the case of over-parameterized networks. A hypothesis is that in the more over-parameterized case, there is a *higher*



proliferation of solutions, including those that fit random labels, in the near vicinity of the networks. As a result, the network parameters have to traverse less (or about the same) in the landscape, resulting in similarly low values of the Lipschitz constant (following Eqn. 3). Despite being a fascinating direction, exploring this hypothesis in extensive detail is beyond the current scope but would however be a fascinating direction for future work. More details on the setup and the upper bound plots are present in Appendices S1.5.13 and S2.8.

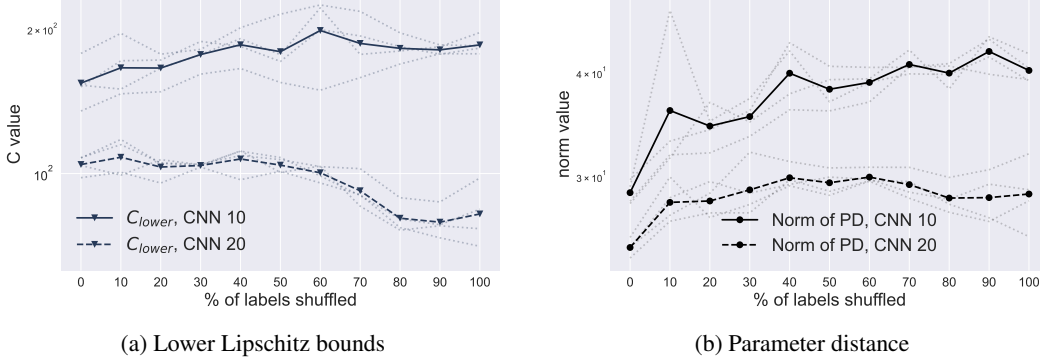


Figure 8: Log plots of Lower Lipschitz values and parameter distance for the last epoch by the amount of label shuffling for **CNN 10 and CNN 20**. Models were trained on a subset of 5000 images from CIFAR-10. Results are averaged over 4 seeds. More details in Appendix S1.5.13.

## 5 Miscellaneous Findings

In our study of Lipschitz constant evolution in Sections 4.1, 4.2 and S2.2 we show the effects of the optimisation procedure on the Lipschitz constant of the network. The current section focuses on examining the effects of choosing the training strategy, in particular, the choice of the loss function and the optimisation algorithm. We also briefly discuss the effects of depth and the number of training samples.

### 5.1 Effect of the loss function: CE vs MSE

Surprisingly, training networks with MSE loss results in marginally lower Lipschitz bounds than in the case of Cross-Entropy, as shown in Figure 9a. We contribute this behaviour to the constraints that MSE imposes on the function output in the case of classification. Since in the MSE scenario an ideal model should output a zero vector with only one entry of value 1, model’s outputs are restricted to unit vectors for the domain of training samples. At the same time, Cross-Entropy loss does not impose this constraint as output logits are implicitly Softmax-ed. Figure 9b shows that applying Softmax to the output of the Cross-Entropy network shrinks the Lipschitz constant dramatically.

### 5.2 Effect of the optimisation algorithm: SGD vs Adam

When a network is trained using the Adam optimiser, Lipschitz constant bounds escalate dramatically compared to the results from SGD. This finding supports the fact that Adam finds solutions that generalise significantly worse, despite great training performance [40, 41]. Note that this trend remains even if we account for Adam’s faster convergence, i.e. compare networks at their respective last epochs of training, which are not the same due to various convergence rates (see Figure 10).

We suggest that this behaviour can be explained by observing how far models travel from their initial parameters. Figure 11 shows the evolution of parameter distances (i.e.  $param\_dist_\tau = \sum_{t=1}^{\tau} \|\theta^t - \theta^{t-1}\|_2$ , where  $t$  iterates through saved model checkpoints), which has a similar trend to Lipschitz bounds. In fact, we show that Lipschitz constant can be indeed expressed in terms of parameter distance in our theoretical analysis in Section S3.1. We leave a thorough exploration of this facet for future work. As a bonus we also show that parameter distance also exhibits Double Descent, see Figure 12.

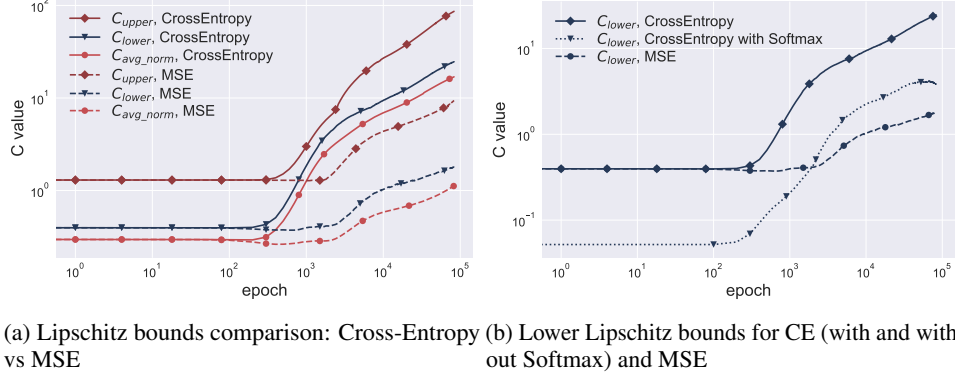


Figure 9: Lipschitz constant bounds evolution for FCN ReLU network with 1 hidden layer with 256 neurons, trained using **Cross-Entropy** and **MSE**. Both models were trained on MNIST1D with SGD, using the same learning rate and LR scheduler. Results are averaged over 4 runs. More details are in Appendix S1.5.9.

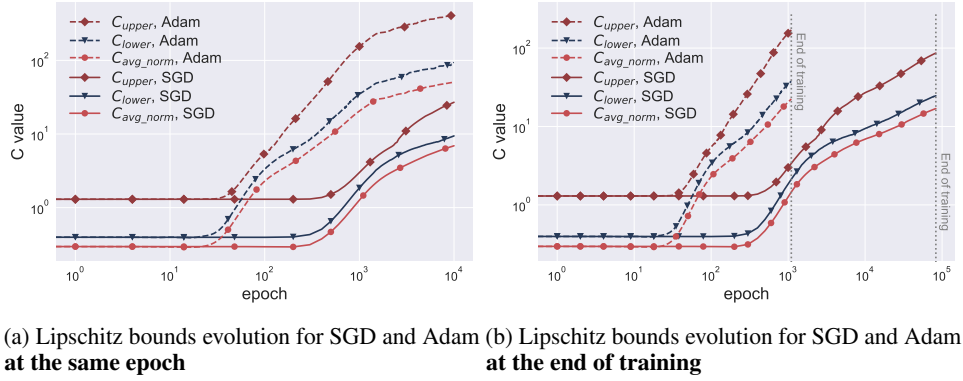


Figure 10: Lipschitz constant bounds evolution for FCN ReLU network with 1 hidden layer with 256 neurons, trained using **SGD** and **Adam**. Both models were trained on MNIST1D with Cross-Entropy loss, using the same LR and LR scheduler. Results are averaged over 4 runs. We end training when the gradient norm reaches the critical value of 0.01. More details are in Appendix S1.5.10.

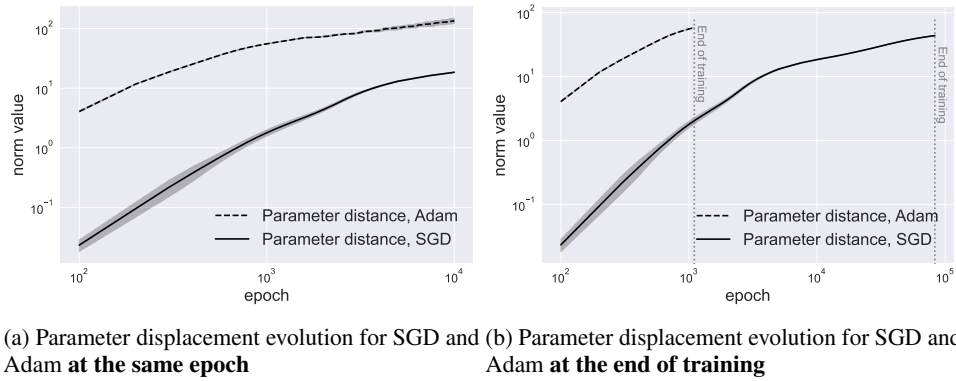


Figure 11: Parameter displacement evolution for FCN ReLU network with 1 hidden layer with 256 neurons, trained using **SGD** and **Adam**. Both models were trained on MNIST1D with Cross-Entropy loss, using the same LR and LR scheduler. Results are averaged over 4 runs. We end training when the gradient norm reaches the critical value of 0.01. More details are in Appendix S1.5.10.

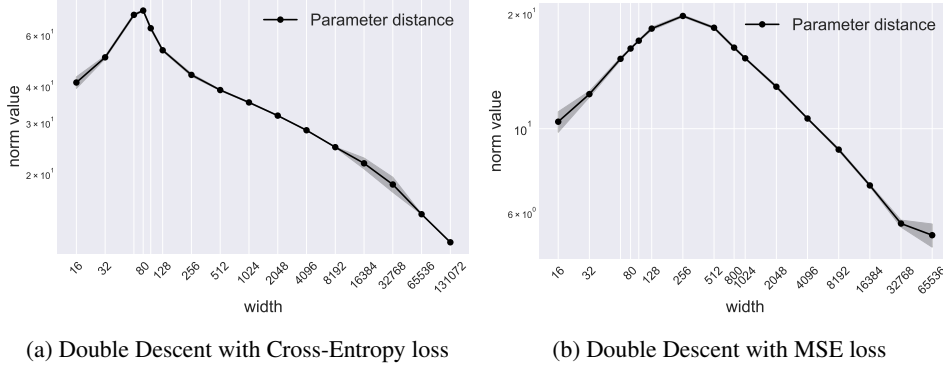


Figure 12: Parameter distance at the last epoch for models from the Double Descent on MNIST1D setting with Cross-Entropy (Fig. 5) and MSE (Fig. S5) losses. More details are in Appendices S1.5.1 and S1.5.2.

### 5.3 Effect of depth

To study how depth affects the Lipschitz constant of the network we trained 5 fully-connected networks on MNIST1D with the same learning parameters. According to Figure 13a, all Lipschitz bounds for trained models start to increase with each subsequent layer after 2 layers, following a trend close to power law —  $R^2$  linear regression metrics are 0.9749, 0.9483 and 0.8798 for upper, lower, and average Lipschitz bounds respectively. The slopes for the corresponding Lipschitz bounds are 3.33, 2.03 and 1.19, indicating a superlinear trend.

An interesting fact is that the aforementioned trend for lower Lipschitz bounds does not hold for networks at initialisation, both for the case of increasing depth (Figure 13b) and increasing width (Figure 15). Consequently, we see how the effect of feature learning gets manifested in the bounds of the Lipschitz constant and that looking solely at initialisation (as in the style of the lazy regime [42]) would be insufficient. To visualise this ‘trend flipping’ behaviour we also present evolution plots for the upper and lower Lipschitz constant bounds in Figure 14.

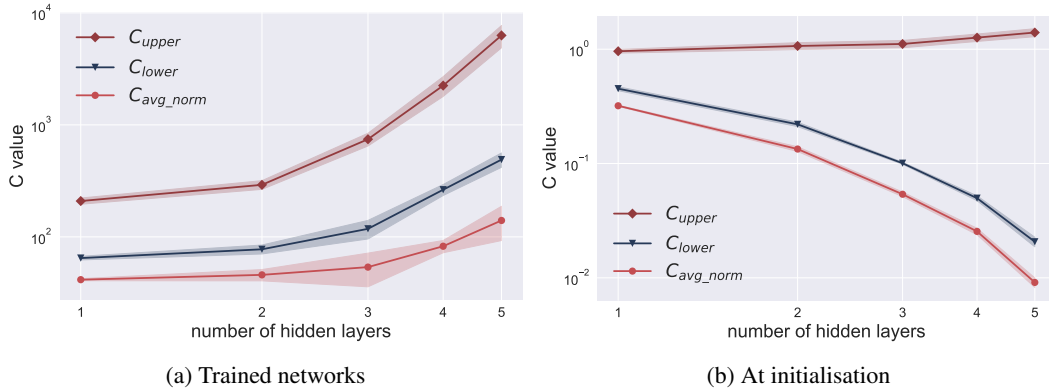


Figure 13: Lipschitz constant bounds for FCN ReLU network with various number of hidden layer with 64 neurons for parameters at initialisation and after training. Results are averaged over 4 runs. More details are in Appendix S1.5.11.

### 5.4 Effect of the number of training samples

Increasing the number of samples in the dataset results in a corresponding sublinear increase in all Lipschitz bounds. Figure 16 shows the Lipschitz bounds for FCN ReLU 256 networks trained on various random subsets of MNIST1D. Using linear regression we estimated the slope of upper, lower and average Lipschitz bounds to be 0.53, 0.37 and 0.36 respectively, and the  $R^2$  metrics are 0.9680, 0.9932 and 0.9928, implying a strong sublinear trend in all Lipschitz bounds. These results suggest

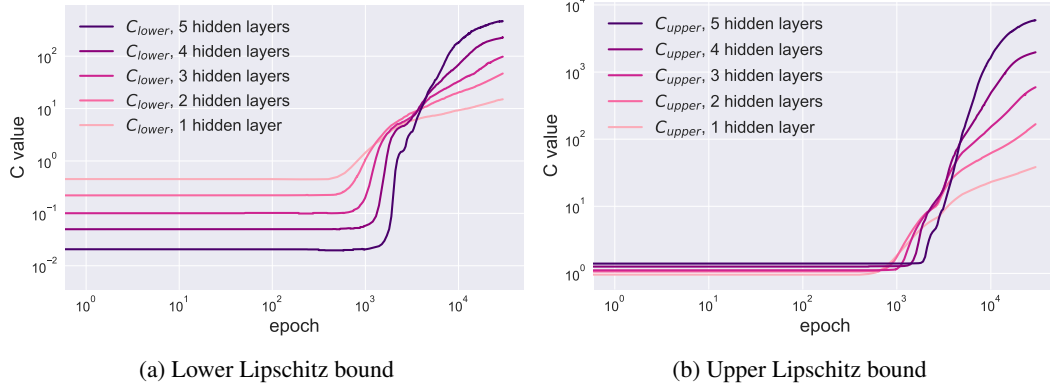


Figure 14: Lipschitz constant bounds evolution for FCN ReLU networks with various number of hidden layer with 64 neurons for parameters. Results are averaged over 4 runs. More details are in Appendix S1.5.11.

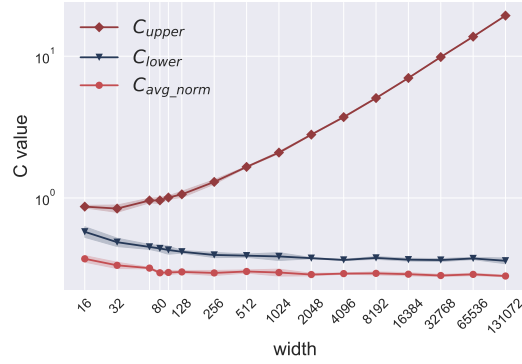


Figure 15: Lipschitz constant bounds for FCN ReLU network with increasing hidden layer width at initialisation. Results are averaged over 4 runs. Here we used models from the Double Descent experiment, see details in Appendix S1.5.1.

that as the number of samples increases, the complexity of the function rises to fit a larger set of points. It would be interesting to precisely tease out this behaviour in terms of relevant theoretical quantities, but we leave that for future work.

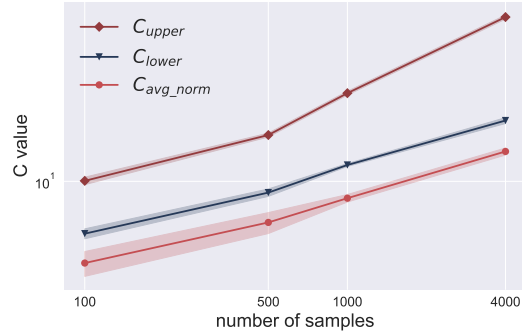


Figure 16: Lipschitz constant bounds for FCN ReLU network with 1 hidden layer with 256 neurons trained for various subsets of MNIST1D. Results are averaged over 4 runs. More details are in Appendix S1.5.12.

## 6 Discussion

*Summary.* To summarise, we have presented a wide-ranging study of the trends of the Lipschitz constant in various learning settings. First, we have shown evolution trends of various Lipschitz constant bounds for different networks, displaying the faithfulness of the simple lower bound with respect to the true Lipschitz constant — even for the unprecedented setting of ResNet50 on ImageNet. Second, we looked at the behaviour of Lipschitz constant in the Double Descent setting and have shown that both lower and upper Lipschitz bounds exhibit trends similar to test loss. We next presented theoretical statements, connecting Lipschitz constant with the variance term in the generalisation bound, and also gave experimental proof to those statements. In the subsequent sections, we discussed the effect of the choice of loss (between Cross-Entropy and MSE), optimisation algorithm (SGD versus Adam), depth of the network and training sample modifications, like label noise.

**Limitations & future research directions.** One potential avenue for investigation is to explore more complex model classes, such as ResNets or different types of Transformers [43]. Additionally, it would be of great interest to compare tighter Lipschitz constant bounds, proposed in the literature, with the results presented in this study. Another promising area for future research is to examine how various forms of input noise affect the Lipschitz constant. In particular, it would be interesting to investigate the fidelity of the lower bounds when accounting for adversarial perturbations, as in adversarial examples [4].

All in all, we hope that this work inspires further research on uncovering and understanding the characteristics of the Lipschitz constant.

## Acknowledgements

We would like to thank Thomas Hofmann, Bernhard Schölkopf, and Aurelien Lucchi for their useful comments and suggestions. We are also grateful to the members of the DALab for their support. Sidak Pal Singh would like to acknowledge the financial support from Max Planck ETH Center for Learning Systems.

## References

- [1] Stuart Geman, Elie Bienenstock, and René Doursat. Neural networks and the bias/variance dilemma. *Neural computation*, 4(1):1–58, 1992.
- [2] Peter Bartlett, Dylan J. Foster, and Matus Telgarsky. Spectrally-normalized margin bounds for neural networks, 2017.
- [3] Tsui-Wei Weng, Huan Zhang, Pin-Yu Chen, Jinfeng Yi, Dong Su, Yupeng Gao, Cho-Jui Hsieh, and Luca Daniel. Evaluating the robustness of neural networks: An extreme value theory approach. In *International Conference on Learning Representations*, 2018. URL <https://openreview.net/forum?id=BkUHLMZOb>.
- [4] Ian J Goodfellow, Jonathon Shlens, and Christian Szegedy. Explaining and harnessing adversarial examples. *arXiv preprint arXiv:1412.6572*, 2014.
- [5] Todd P. Huster, Cho-Yu Jason Chiang, and Ritu Chadha. Limitations of the lipschitz constant as a defense against adversarial examples. *ArXiv*, abs/1807.09705, 2018.
- [6] Matt Jordan and Alexandros G Dimakis. Exactly computing the local lipschitz constant of relu networks. *Advances in Neural Information Processing Systems*, 33:7344–7353, 2020.
- [7] Kevin Scaman and Aladin Virmaux. Lipschitz regularity of deep neural networks: analysis and efficient estimation. In *Neural Information Processing Systems*, 2018.
- [8] Kaidi Xu, Zhouxing Shi, Huan Zhang, Yihan Wang, Kai-Wei Chang, Minlie Huang, Bhavya Kailkhura, Xue Lin, and Cho-Jui Hsieh. Automatic perturbation analysis for scalable certified robustness and beyond. *Advances in Neural Information Processing Systems*, 33:1129–1141, 2020.
- [9] Mahyar Fazlyab, Alexander Robey, Hamed Hassani, Manfred Morari, and George J. Pappas. Efficient and accurate estimation of lipschitz constants for deep neural networks. In *Neural Information Processing Systems*, 2019.



- [10] Fabian Latorre Gómez, Paul Rolland, and Volkan Cevher. Lipschitz constant estimation of neural networks via sparse polynomial optimization. *CoRR*, abs/2004.08688, 2020. URL <https://arxiv.org/abs/2004.08688>.
- [11] Cem Anil, James Lucas, and Roger Baker Grosse. Sorting out lipschitz function approximation. In *International Conference on Machine Learning*, 2018.
- [12] Henry Gouk, Eibe Frank, Bernhard Pfahringer, and Michael J. Cree. Regularisation of neural networks by enforcing lipschitz continuity. *Machine Learning*, 110(2):393–416, Feb 2021. ISSN 1573-0565. doi: 10.1007/s10994-020-05929-w. URL <https://doi.org/10.1007/s10994-020-05929-w>.
- [13] Moustapha Cissé, Piotr Bojanowski, Edouard Grave, Yann Dauphin, and Nicolas Usunier. Parseval networks: Improving robustness to adversarial examples. *ArXiv*, abs/1704.08847, 2017.
- [14] Henning Petzka, Asja Fischer, and Denis Lukovnikov. On the regularization of wasserstein gans. *ArXiv*, abs/1709.08894, 2017.
- [15] Yusuke Tsuzuku, Issei Sato, and Masashi Sugiyama. Lipschitz-margin training: Scalable certification of perturbation invariance for deep neural networks. In S. Bengio, H. Wallach, H. Larochelle, K. Grauman, N. Cesa-Bianchi, and R. Garnett, editors, *Advances in Neural Information Processing Systems*, volume 31. Curran Associates, Inc., 2018. URL <https://proceedings.neurips.cc/paper/2018/file/485843481a7edacbfce101ecb1e4d2a8-Paper.pdf>.
- [16] Mikhail Belkin, Daniel J. Hsu, Siyuan Ma, and Soumik Mandal. Reconciling modern machine-learning practice and the classical bias–variance trade-off. *Proceedings of the National Academy of Sciences*, 116: 15849 – 15854, 2019.
- [17] Aladin Virmaux and Kevin Scaman. Lipschitz regularity of deep neural networks: analysis and efficient estimation. In S. Bengio, H. Wallach, H. Larochelle, K. Grauman, N. Cesa-Bianchi, and R. Garnett, editors, *Advances in Neural Information Processing Systems*, volume 31. Curran Associates, Inc., 2018. URL <https://proceedings.neurips.cc/paper/2018/file/d54e99a6c03704e95e6965532dec148b-Paper.pdf>.
- [18] Sébastien Bubeck and Mark Sellke. A universal law of robustness via isoperimetry. *Journal of the ACM*, 70:1 – 18, 2021.
- [19] N. Benjamin Erichson, Omri Azencot, A. F. Queiruga, and Michael W. Mahoney. Lipschitz recurrent neural networks. *ArXiv*, abs/2006.12070, 2020.
- [20] Qiyang Li, Saminul Haque, Cem Anil, James Lucas, Roger B Grosse, and Jörn-Henrik Jacobsen. Preventing gradient attenuation in lipschitz constrained convolutional networks. *Advances in neural information processing systems*, 32, 2019.
- [21] Hyunjik Kim, George Papamakarios, and Andriy Mnih. The lipschitz constant of self-attention. In *International Conference on Machine Learning*, 2020.
- [22] Zhiming Zhou, Jiadong Liang, Yuxuan Song, Lantao Yu, Hongwei Wang, Weinan Zhang, Yong Yu, and Zhihua Zhang. Lipschitz generative adversarial nets. *CoRR*, abs/1902.05687, 2019. URL <http://arxiv.org/abs/1902.05687>.
- [23] Max Revay, Ruigang Wang, and Ian R. Manchester. Lipschitz bounded equilibrium networks. *ArXiv*, abs/2010.01732, 2020.
- [24] Kavosh Asadi, Dipendra Kumar Misra, and Michael L. Littman. Lipschitz continuity in model-based reinforcement learning. In *International Conference on Machine Learning*, 2018.
- [25] Leon Bungert, René Raab, Tim Roith, Leo Schwinn, and Daniel Tenbrinck. Clip: Cheap lipschitz training of neural networks. In *Scale Space and Variational Methods in Computer Vision*, 2021.
- [26] Yujia Huang, Huan Zhang, Yuanyuan Shi, J. Zico Kolter, and Anima Anandkumar. Training certifiably robust neural networks with efficient local lipschitz bounds. In *Neural Information Processing Systems*, 2021.
- [27] Patricia Pauli, Anne Koch, Julian Berberich, Paul Kohler, and Frank Allgöwer. Training robust neural networks using lipschitz bounds. *2021 American Control Conference (ACC)*, pages 2595–2600, 2021.
- [28] Hajime Ono, Tsubasa Takahashi, and Kazuya Kakizaki. Lightweight lipschitz margin training for certified defense against adversarial examples. *ArXiv*, abs/1811.08080, 2018.

- [29] Yipeng Qin, Niloy Jyoti Mitra, and Peter Wonka. How does lipschitz regularization influence gan training? In *European Conference on Computer Vision*, 2018.
- [30] Zhiming Zhou, Yuxuan Song, Lantao Yu, and Yong Yu. Understanding the effectiveness of lipschitz constraint in training of gans via gradient analysis. *ArXiv*, abs/1807.00751, 2018.
- [31] Shaobo Cui and Yong Jiang. Effective lipschitz constraint enforcement for wasserstein gan training. *2017 2nd IEEE International Conference on Computational Intelligence and Applications (ICCI)*, pages 74–78, 2017.
- [32] Dávid Terjék. Adversarial lipschitz regularization. In *International Conference on Learning Representations*, 2019.
- [33] Matteo Gamba, Hossein Azizpour, and Marten Bjorkman. On the lipschitz constant of deep networks and double descent. *ArXiv*, abs/2301.12309, 2023.
- [34] Mikhail Belkin, Daniel J. Hsu, Siyuan Ma, and Soumik Mandal. Reconciling modern machine-learning practice and the classical bias–variance trade-off. *Proceedings of the National Academy of Sciences*, 116: 15849 – 15854, 2019.
- [35] Herbert Federer. *Geometric Measure Theory*, chapter 3.1.1, page 209. Springer Berlin, Heidelberg, 1 edition, 1996.
- [36] Sam Greydanus. Scaling \*down\* deep learning. *CoRR*, abs/2011.14439, 2020. URL <https://arxiv.org/abs/2011.14439>.
- [37] Sidak Pal Singh, Aurelien Lucchi, Thomas Hofmann, and Bernhard Schölkopf. Phenomenology of double descent in finite-width neural networks, 2022. URL <https://arxiv.org/abs/2203.07337>.
- [38] Ben Adlam and Jeffrey Pennington. The neural tangent kernel in high dimensions: Triple descent and a multi-scale theory of generalization, 2020.
- [39] Chiyuan Zhang, Samy Bengio, Moritz Hardt, Benjamin Recht, and Oriol Vinyals. Understanding deep learning (still) requires rethinking generalization. *Communications of the ACM*, 64(3):107–115, 2021.
- [40] Ashia C. Wilson, Rebecca Roelofs, Mitchell Stern, Nathan Srebro, and Benjamin Recht. The marginal value of adaptive gradient methods in machine learning. In *NIPS*, 2017.
- [41] Yizhou Wang, Yue yue Kang, Can Qin, Yi Xu, Huan Wang, Yulun Zhang, and Yun Raymond Fu. Adapting stepsizes by momentumized gradients improves optimization and generalization. *ArXiv*, abs/2106.11514, 2021.
- [42] Lenaic Chizat, Edouard Oyallon, and Francis Bach. On lazy training in differentiable programming. arxiv e-prints, page. *arXiv preprint arXiv:1812.07956*, 2018.
- [43] Ashish Vaswani, Noam M. Shazeer, Niki Parmar, Jakob Uszkoreit, Llion Jones, Aidan N. Gomez, Lukasz Kaiser, and Illia Polosukhin. Attention is all you need. *ArXiv*, abs/1706.03762, 2017.
- [44] Ian Goodfellow, Yoshua Bengio, and Aaron Courville. *Deep Learning*, chapter 9.1, page 329. MIT Press, 2016. <http://www.deeplearningbook.org>.
- [45] Preetum Nakkiran, Gal Kaplun, Yamini Bansal, Tristan Yang, Boaz Barak, and Ilya Sutskever. Deep double descent: Where bigger models and more data hurt, 2019.
- [46] Alex Krizhevsky. Learning multiple layers of features from tiny images. 2009.
- [47] Yerlan Idelbayev. Proper ResNet implementation for CIFAR10/CIFAR100 in PyTorch. [https://github.com/akamaster/pytorch\\_resnet\\_cifar10](https://github.com/akamaster/pytorch_resnet_cifar10). Accessed: 2023-06-17.
- [48] Brady Neal, Sarthak Mittal, Aristide Baratin, Vinayak Tania, Matthew Scicluna, Simon Lacoste-Julien, and Ioannis Mitliagkas. A modern take on the bias-variance tradeoff in neural networks, 2018.

# Appendix

## Table of Contents

---

<b>S1 Experimental setup</b>	<b>17</b>
S1.1 Upper bound calculation . . . . .	17
S1.2 Model descriptions . . . . .	18
S1.3 Training strategy . . . . .	19
S1.4 LR Schedulers . . . . .	19
S1.5 Description of experimental settings . . . . .	20
<b>S2 Additional experiments</b>	<b>23</b>
S2.1 Estimation of the potential error of evaluating lower Lipschitz bound by considering a subsample of ImageNet . . . . .	23
S2.2 Lipschitz evolution for other settings . . . . .	23
S2.3 Lipschitz Double Descent for other settings . . . . .	26
S2.4 More experiments on the Lipschitz constant in the Double Descent setting . . . . .	27
S2.5 Bias-Variance trade-off evaluation . . . . .	27
S2.6 Optimising the upper bound for the Variance . . . . .	27
S2.7 Variance bounds for the complete sweep of widths . . . . .	28
S2.8 More experiments on the effect of label noise . . . . .	28
S2.9 ResNet50 upper bound on more checkpoints . . . . .	30
S2.10 Jacobian norm distributions for other models and datasets. . . . .	30
<b>S3 Theoretical proofs</b>	<b>32</b>
S3.1 Theoretical analysis of Lipschitz evolution . . . . .	32
S3.2 Bias-Variance tradeoff . . . . .	33

---

## S1 Experimental setup

This section contains comprehensive details on the experiments in the paper — this includes a summary of our strategy for Lipschitz upper bound calculation, models’ architecture descriptions, hyperparameters and optimisation strategy choices for every experimental section in the main and supplementary parts of the paper.

All plots with shaded regions represent an uncertainty of  $\pm$  standard deviation from the mean, which is computed across different seeds. When semi-transparent dotted lines are shown, the solid line represents the mean over seeds and each dotted line depicts data from individual seeds.

### S1.1 Upper bound calculation

We start by describing our approach to computing the upper bound of the Lipschitz constant, inspired by the AutoLip algorithm introduced by [17]. As briefly discussed in the main part of the paper (Section 3), we simply multiply per-layer Lipschitz bounds. For network  $f_{\theta}$  with  $L$  layers, defined as  $f_{\theta} := f^{(L)} \circ \sigma \circ f^{(L-1)} \circ \sigma \circ \dots \circ f^{(1)}$ , where  $\sigma$  is a 1-Lipschitz non-linear activation function, the upper bound looks as follows:

$$C \leq \prod_{i=1}^L \sup_{\mathbf{x}^{(i-1)} \in \text{dom}(f^{(i)})} \|\nabla_{\mathbf{x}^{(i-1)}} f^{(i)}\| \leq \prod_{i=1}^L \sup \|\nabla_{\mathbf{x}^{(i-1)}} f^{(i)}\| =: C_{\text{upper}} \quad (2)$$

More pedantically, one can see this by using Theorem 3.1 and applying the chain rule:

$$\begin{aligned} C &= \sup_{\mathbf{x} \in \text{dom}(f_{\theta})} \|\nabla_{\mathbf{x}} f_{\theta}\| = \sup_{\mathbf{x} \in \text{dom}(f_{\theta})} \|\nabla_{f^{(L-1)}} f^{(L)} \cdot \nabla_{f^{(L-2)}} f^{(L-1)} \cdot \dots \cdot \nabla_{f^{(1)}} f^{(2)} \cdot \nabla_{\mathbf{x}} f^{(1)}\| \\ &\leq \sup_{f^{(L-1)}(\mathbf{x})} \|\nabla_{f^{(L-1)}} f^{(L)}\| \cdot \dots \cdot \sup_{f^{(1)}(\mathbf{x})} \|\nabla_{f^{(1)}} f^{(2)}\| \cdot \sup_{\mathbf{x} \in \text{dom}(f_{\theta})} \|\nabla_{\mathbf{x}} f^{(1)}\| \\ &\leq \sup \|\nabla_{f^{(L-1)}} f^{(L)}\| \cdot \dots \cdot \sup \|\nabla_{f^{(1)}} f^{(2)}\| \cdot \sup \|\nabla_{\mathbf{x}} f^{(1)}\| =: C_{\text{upper}}, \end{aligned} \quad (4)$$

where in the last line we consider the unconstrained supremum.

**Linear operations.** Each linear layer of the form  $f^{(i)}(\mathbf{x}) = \mathbf{W}^{(i)} \mathbf{x}$  has Lipschitz constant  $\|\mathbf{W}^{(i)}\|_2$ , since the Jacobian of  $f^{(i)}$  is simply the weight matrix. Convolutional layers are also linear operators and therefore can be similarly expressed as a linear transformation (considering that we perform proper flattening of the input image and reshaping in the end). According to Goodfellow et. al. [44], equivalent linear transformations are represented by doubly block Toeplitz matrices which only depend on kernel weights. At the same time, Batch Normalisation layers are also per-feature linear transformations and, thus, the upper bound can be calculated as a maximum across per-feature Lipschitz constants.

**Activation functions.** All activation functions that are used in this paper — ReLU, Leaky ReLU with slope 0.01, max and average pooling — are also at most 1-Lipschitz and thus are considered 1-Lipschitz for the upper bound computation.

**Residual layers.** Residual layers of the form  $f(\mathbf{x}) = g(\mathbf{x}) + \mathbf{x}$ , where  $f, g : \mathbb{R}^n \rightarrow \mathbb{R}^n$  and  $g$  is  $C_g$ -Lipschitz continuous, simply have a Lipschitz constant equal to  $C_f = C_g + 1$ . One can trivially derive this using the definition of Lipschitz continuity and the triangle inequality:

$$\begin{aligned} \|f(\mathbf{x}) - f(\mathbf{y})\| &= \|g(\mathbf{x}) - g(\mathbf{y}) + \mathbf{x} - \mathbf{y}\| \\ &\leq \|g(\mathbf{x}) - g(\mathbf{y})\| + \|\mathbf{x} - \mathbf{y}\| && \text{(Triangle inequality)} \\ &\leq C_g \|\mathbf{x} - \mathbf{y}\| + \|\mathbf{x} - \mathbf{y}\| \\ &= (C_g + 1) \|\mathbf{x} - \mathbf{y}\| \end{aligned} \quad (5)$$

*Remark on computational challenges.* Since equivalent linear weight matrices for convolutional operations assume flat input, the dimensions of this matrix grow rapidly with increasing image size and channel depth. This results in large memory consumption, which we leveraged by converting this

matrix into the `scipy` sparse CSR format and using `scipy.sparse.linalg` library to compute the norm. We also found that standard `pytorch` implementation of 2-norm computation works rather slowly for large matrices. We have therefore implemented a Power method to compute 2-norms for linear layers and batched Jacobian matrices, resulting in almost  $10\times$  speedup in some cases.

## S1.2 Model descriptions

### S1.2.1 FCN ReLU networks

A fully Connected Network with ReLU activations (or FCN ReLU for short) consists of a sequence of Linear layers with zero bias term, each followed by a ReLU activation layer, the last layer included. When it is specified that FCN ReLU has a width of 256, there are only two linear transformations involved: first, from an input vector to a hidden vector of size 256, and second, from a hidden layer of size 256 to the output dimension. When a sequence of widths is given (i.e. FCN ReLU with widths 64,64), FCN has several hidden layers, sizes of which are listed from the hidden layer closer to the input to the hidden layer closer to the output.

*Remark on the Dead ReLU problem.* Since we use ReLU as the last layer’s activation, outputs of the model can in some cases become zero-vectors, specifically in scenarios with classification using MSE loss. To address this issue we use a modified version of the FCN model for all MSE experiments — the last ReLU activation is substituted with a Leaky ReLU function with a negative slope of 0.01.

Table S1 shows a list of FCN ReLU realisations with various hidden layer widths and depths and the respective number of model parameters. All models in this table are configured for the MNIST1D<sup>S1</sup> dataset.

Model name	Number of parameters
FCN ReLU 16	800
FCN ReLU 32	1,600
⋮	⋮
FCN ReLU 80	4,000
⋮	⋮
FCN ReLU 256	12,800
⋮	⋮
FCN ReLU 800	40,000
⋮	⋮
FCN ReLU 131072	6,553,600
FCN ReLU 64,64	7,296
FCN ReLU 64,64,64	11,392
FCN ReLU 64,64,64,64	15,488
FCN ReLU 64,64,64,64,64	19,584

Table S1: Table of the number of parameters of FCN ReLU models of various widths and depths, configured for the MNIST1D dataset.

### S1.2.2 CNN networks

Our version of Convolutional Neural Networks (or CNNs for short) follows an approach similar to [45]. We consider a 5-layer model, with 4 Conv-ReLU-MaxPool blocks, followed by a Linear layer with zero bias. All convolution layers have  $3 \times 3$  kernels with `stride=1`, `padding=1` and zero bias. Kernel output channels for convolution layers follow the pattern  $[w, 2w, 4w, 8w]$ , where  $w$  is the width of the model. Meanwhile, MaxPooling layers have kernels of sizes  $[1, 2, 2, 8]$  for the case

<sup>S1</sup>MNIST1D input image is a vector of size 40.



of CIFAR-10<sup>S2</sup> and [1, 2, 2, 7] for the case of MNIST<sup>S3</sup>. This configuration shrinks the input image to a single vector that is then passed to the last Linear layer, yielding the output vector of size 10.

Table S2 displays a list of CNN realisations with various hidden layer widths and the respective number of model parameters. Since configurations for CIFAR-10 [46] and MNIST differ only in the MaxPooling layer size, the number of trainable parameters remains the same for both datasets.

Model name	Number of parameters
CNN 5	9,985
CNN 7	19,271
CNN 10	38,870
CNN 11	46,915
CNN 12	55,716
CNN 13	65,273
⋮	⋮
CNN 20	153,340
⋮	⋮
CNN 60	1,367,220

Table S2: Table of the number of parameters of the CNN network of various widths.

### S1.3 Training strategy

We present experiments that compare models that have a substantially varying number of parameters. To minimise the effect of variability in training, we painstakingly enforce the same learning rate, batch size and optimiser configuration for all models in one sweep. While this choice makes our claims on the behaviour of the Lipschitz constant stronger, we now have the challenge of setting a reasonable stopping criterion to manage variable convergence rates.

For model  $f_{\theta}$  with parameter vector  $\theta$  and loss on the training set  $\mathcal{L}(\theta, S)$ , after the end of each epoch we compute  $\|\nabla_{\theta} \mathcal{L}(\theta, S)\|_2$ , which we call gradient norm for simplicity. In all experiments, unless stated otherwise, we control model training by monitoring the respective gradient norm — if it reaches a small value (ideally zero), our model has negligible parameter change (i.e.  $\|\theta^{t+1} - \theta^t\|_2$  is small) or, in other words, has reached a local minimum. By means of experimentation, we found that stopping models at 0.01 gradient norm value gives good results for most scenarios.

*Possible pitfalls.* In most cases, during the course of training, the gradient norm is at first relatively small (in the range of  $10^{-4}$  to  $10^{-2}$ ), then rapidly increases and then slowly decreases. If our only stopping criteria is minuscule gradient norm, we may end up early stopping models right after a few epochs. To avoid this we also introduce a minimum number of epochs that each model has to train for.

### S1.4 LR Schedulers

This section thoroughly describes learning rate schedulers (LR schedulers for short) that we use in our experiments. Each scheduler modifies a variable  $\gamma_t$ , which is a coefficient that is multiplied by some base learning rate (i.e. learning rate at time step  $t$  is  $\eta_t = \gamma_t \cdot \eta$ , where  $\eta$  is the base learning rate). Note that we perform scheduler updates at every parameter update (which happens several times per epoch), and the schedulers are aware of the dataset length and batch size to adapt to epoch-based settings accordingly.

**Warmup20000Step25 LR Scheduler (Figure S1a).** This scheduler linearly scales the learning rate from a factor of  $\frac{1}{20,000}$  to 1 for 20,000 updates. Next, the scaling coefficient drops by a factor of

<sup>S2</sup>CIFAR-10 dataset input image has shape  $32 \times 32 \times 3$ .

<sup>S3</sup>MNIST dataset input image has shape  $28 \times 28 \times 3$ .

0.75 every 25% of the next 10,000 epochs. Afterwards, the coefficient remains at the constant factor of  $0.75^3 = 0.421875$ .

**Cont100 LR Scheduler (Figure S1b).** This scheduler continuously drops the scaling coefficient by a factor of 0.95 every 100 epochs.

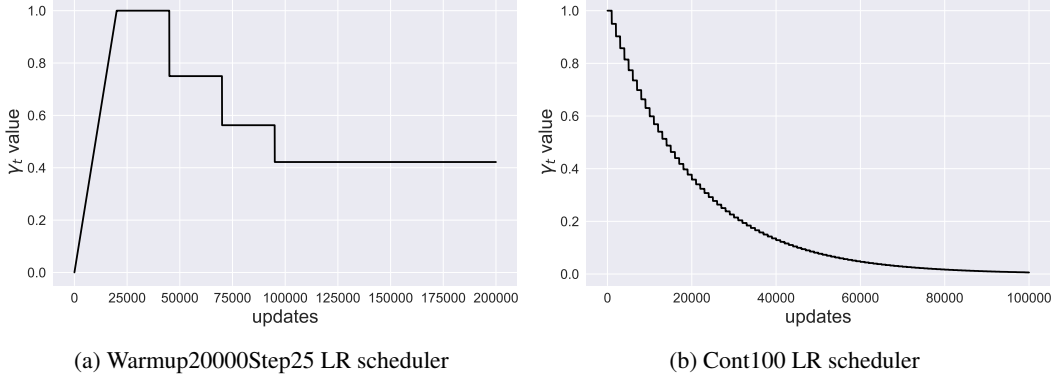


Figure S1: Learning rate scaling coefficient  $\gamma_t$  against updates for two different learning rate schedulers. In each case there are 10 updates per epoch.

## S1.5 Description of experimental settings

This section presents a detailed description of each experimental setup. We also include theoretical Double Descent interpolation thresholds for Double Descent experiments, where in each equation  $n$  stands for the number of training samples,  $K$  for the number of classes and  $p$  for the number of parameters in the model.

### S1.5.1 Double Descent on MNIST1D, FCN ReLU networks, Cross-Entropy loss (Figure 5)

For this experiment, we trained a sweep of FCN ReLU models (see S1.2.1) with widths [16, 32, 64, 80, 96, 128, 256, 512, 1024, 2048, 4096, 8192, 16384, 32768, 65536, 131072] on MNIST1D<sup>S4</sup> with batch size 512 using Cross-Entropy loss and SGD optimiser without momentum. We used a Warmup20000Step25 LR scheduler (see S1.4) and a base learning rate of 0.005. We trained our models for at least 10,000 epochs and stopped each model when either 0.01 gradient norm is reached or when 300,000 epochs have passed. We trained 4 seeds for each run. The theoretical threshold for this scenario is at  $n \approx p$ , which corresponds to FCN ReLU 80 (4000 parameters).

*Comment on the hyperparameter choice.* In this experiment, we used a very small learning rate to smoothly fit both under- and overparametrised models. Therefore we require a significant amount of training epochs to secure convergence for all settings.

*Comment on Figure 5.* In the figure, the training loss uncertainty for models from width 8192 to 65536 is lower bounded by zero (since training loss cannot be negative) and therefore is depicted as a vertical line in the log-log plot.

### S1.5.2 Double Descent on MNIST1D, FCN ReLU networks, MSE loss (Figure S5)

This experiment depicts a sweep of FCN ReLU models (see S1.2.1) with widths [16, 32, 64, 96, 128, 256, 512, 800, 1024, 2048, 4096, 8192, 16384, 32768, 65536], trained on MNIST1D with batch size 512 using MSE loss and SGD optimiser without momentum. We used a Warmup20000Step25 LR scheduler (see S1.4) and a base learning rate of 0.001. We trained our models for at least 10,000 epochs and stopped each model when 0.01 gradient norm is reached or when 200,000 epochs have passed. We trained 4 seeds for each run. The theoretical threshold for this scenario is at  $n \cdot K \approx p$ , which corresponds to FCN ReLU 800 (40,000 parameters).

<sup>S4</sup>MNIST1D has 4000 training samples.

### S1.5.3 Double Descent on CIFAR-10, CNN networks, Cross-Entropy loss (Figure 6)

For this experiment, we trained a sweep of CNN models with widths [5, 7, 10, 11, 12, 15, 20, 25, 30, 35, 40, 45, 50, 55, 60] on CIFAR-10<sup>S5</sup> with batch size 128 using Cross-Entropy loss and SGD optimiser without momentum. We used a Cont100 LR scheduler (see S1.4) and a base learning rate of 0.01. We trained our models for at least 500 epochs and stopped each model when 0.01 gradient norm is reached or when 5000 epochs have passed. We trained 4 seeds for each run. The theoretical threshold for this scenario is at  $n \approx p$ , which corresponds to somewhere between CNN 11 (46,915 parameters) and CNN 12 (55,716 parameters).

### S1.5.4 Double Descent on MNIST, CNN networks, Cross-Entropy loss (Figure S6)

For this experiment, we trained a sweep of CNN models with widths [5, 7, 10, 11, 12, 13, 15, 20, 25, 30, 35, 40, 45, 50, 55, 60] on MNIST<sup>S6</sup> with a fixed 10% label shuffling (i.e. the dataset is the same across all seeds and models) with batch size 128 using Cross-Entropy loss and SGD optimiser without momentum. We used a Cont100 LR scheduler (see S1.4) and a base learning rate of 0.01. We trained our models for at least 100 epochs and stopped each model when 0.01 gradient norm is reached or when 1000 epochs. We train 4 seeds for each run. The theoretical threshold for this scenario is at  $n \approx p$ , which corresponds to somewhere between CNN 12 (55,716 parameters) and CNN 13 (65,273 parameters).

### S1.5.5 Lipschitz bounds evolution, FCN ReLU, MNIST1D with convex combinations (Fig. 2)

To showcase Lipschitz constant evolution we trained 4 FCN ReLU 256 with different seeds on the MNIST1D dataset with batch size 512 for 83,000 epochs. Models were trained using Cross-Entropy loss and SGD optimiser with a base learning rate of 0.005 and Warmup20000Step25 LR scheduler (see S1.4). Each model achieved gradient norm of 0.01 up to 2 significant figures. Each epoch consists of 8 parameter updates.

For this scenario, we empirically defined the stable phase to begin from epoch 2500 (or after 20,000 updates). The slopes for the upper, lower, and average Lipschitz bounds are: 0.59, 0.46 and 0.44 respectively and are computed by examining the slope coefficient of a linear regression model fitted to the corresponding values in the log-log scale. The  $R^2$  values of the fit for the upper, lower, and average Lipschitz bounds are 0.9955, 0.9986 and 0.9980 respectively.

To compute the lower bound on convex combinations of samples from MNIST1D we constructed a set  $S^*$ , which contains: (a) training set  $S$  — 4000 samples, (b) test set  $S'$  — 1000 samples, (c) convex combinations  $\lambda \mathbf{x}_i + (1 - \lambda) \mathbf{x}_j$  from  $S$  — 100,000 samples for each  $\lambda = \{0.1, 0.2, 0.3, 0.4, 0.5\}$ , and (d) convex combinations  $\lambda \mathbf{x}_i + (1 - \lambda) \mathbf{x}_j$  from  $S'$  — 100,000 samples for each  $\lambda = \{0.1, 0.2, 0.3, 0.4, 0.5\}$ . Altogether this makes  $S^*$  contain 1,005,000 samples.

### S1.5.6 Lipschitz bounds evolution, ResNet50, subset of 200,000 ImageNet samples (Figure 3)

For this experiment, we trained 3 ResNet50 models with different seeds for 90 epochs on full ImageNet with batch size 256, using Cross-Entropy loss and SGD optimiser with momentum of 0.9, weight decay of 0.0001 and base learning rate 0.1. We also used a LR decay scheme where the learning rate is decreased 10 times every 30 epochs. We then evaluated lower Lipschitz bounds for epochs [0, 1, 10, 20, 30, 40, 50, 60, 70, 80, 90] on a fixed random subset of 200,000 images from the ImageNet training set. During Lipschitz evaluation, all training samples are resized to  $256 \times 256 \times 3$ , then center-cropped to size  $224 \times 224 \times 3$  and then normalised using  $mean = [0.485, 0.456, 0.406]$  and  $std = [0.229, 0.224, 0.225]$ . During training, training samples are randomly resized and cropped to  $224 \times 224 \times 3$  and then normalised using the same  $mean$  and  $std$ .

For this scenario, we empirically defined the stable phase to begin from epoch 60. The slopes for the upper, lower, and average Lipschitz bounds are: 7.32, 0.49 and 0.48 respectively and are computed by examining the slope coefficient of a linear regression model fitted to the corresponding values in the log-log scale. The  $R^2$  values of the fit for the upper, lower, and average Lipschitz bounds are 0.8441, 0.9718 and 0.8774 respectively.

<sup>S5</sup>CIFAR-10 has 50,000 training samples.

<sup>S6</sup>MNIST has 60,000 training samples.

### S1.5.7 Distribution of the norm of the per-sample Jacobian for ResNet18 trained on ImageNet (Figure 4)

For this experiment we first evaluated the norms of the Jacobian matrices (see 3.1) of ResNet18 for each sample of ImageNet. We took a pretrained ResNet18 from [pytorch hub](#). We then constructed another dataset, which took a mean of all possible pairs of 1,000 ImageNet samples with the highest Jacobian norm from the previous calculation, and evaluated the distribution once more on the new dataset.

### S1.5.8 Variance upper bounds and Bias-Variance tradeoff (Sections 4.3 and S2.5)

For this study we used the same models that we have trained for the Double Descent on MNIST1D using FCN ReLU networks trained with MSE setting (see S1.5.2).

To compute variance bound estimates (see Eq. [Var bound 1](#)) in Figure 7, all expectations and variances are computed as their respective unbiased statistical estimates over 4 seeds.  $\bar{C}$  is estimated as the norm of the average Jacobian among 4 seeds on the training set:

$$\begin{aligned}\bar{C} &= \sup_{\mathbf{x} \in \mathcal{D}} \|\nabla_{\mathbf{x}} \overline{f_{\boldsymbol{\theta}}(\mathbf{x})}\| = \sup_{\mathbf{x} \in \mathcal{D}} \|\nabla_{\mathbf{x}} \mathbb{E}_{\zeta}[f_{\boldsymbol{\theta}}(\mathbf{x}, \zeta)]\| = \sup_{\mathbf{x} \in \mathcal{D}} \|\mathbb{E}_{\zeta}[\nabla_{\mathbf{x}} f_{\boldsymbol{\theta}}(\mathbf{x}, \zeta)]\| \\ &\geq \sup_{\mathbf{x} \in \mathcal{S}} \|\mathbb{E}_{\zeta}[\nabla_{\mathbf{x}} f_{\boldsymbol{\theta}}(\mathbf{x}, \zeta)]\| \approx \sup_{\mathbf{x} \in \mathcal{S}} \left\| \frac{1}{4} \sum_{i=1}^4 (\nabla_{\mathbf{x}} f_{\boldsymbol{\theta}}(\mathbf{x}, \zeta_i)) \right\| \quad (6)\end{aligned}$$

### S1.5.9 Effect of the loss function on the Lipschitz constant (Section 5.1)

For this study we used the same models that we have trained for the Double Descent on MNIST1D using FCN ReLU networks trained with Cross-Entropy setting (see S1.5.1) and with MSE setting (see S1.5.2). We plotted the evolution for the first 83,000 epochs for all models.

### S1.5.10 Effect of the optimisation algorithm on the Lipschitz constant (Section 5.2)

For this study, we used the same models that we have trained for the Double Descent on MNIST1D using FCN ReLU networks trained with Cross-Entropy setting (see S1.5.1), as well as a set of 4 additionally trained FCN ReLU models with various seeds that were optimised with standard pytorch Adam optimiser ( $\beta_1 = 0.9, \beta_2 = 0.999$ ). Each of these models was trained on MNIST1D with Cross-Entropy loss, 0.005 learning rate and Warmup20000Step25 LR scheduler (see S1.4). Parameter vector was computed as a concatenation of flattened layer weights at each layer.

In Figure 10a we showcase models up to epoch 10,000, while in figure 10b models are stopped at 83,000 and 1,100 epochs for the SGD and Adam case respectively. In the former plot, both models achieved a gradient norm of at most 0.01 up to 2 significant figures at the end of their training.

*Comment on Figure 10a.* We display training up to 10,000 epochs even though Adam reached low gradient norm much earlier due to slower rate of SGD — by 1,100 epochs SGD is still in the early training phase.

### S1.5.11 Effect of depth of the network on its Lipschitz constant (Section 5.3)

For this experiment we trained 5 types of FCN ReLU models with increasing depth. In particular, we considered FCN ReLU 64; FCN ReLU 64,64; FCN ReLU 64,64,64; FCN ReLU 64,64,64,64 and FCN ReLU 64,64,64,64,64. Each model was trained on MNIST1D with batch size 512 using Cross-Entropy loss and the SGD optimiser, 0.005 learning rate and Warmup20000Step25 LR scheduler (see S1.4). We trained our models for at least 10,000 epochs and stopped each model when either 0.01 gradient norm is reached or when 300,000 epochs have passed. We trained 4 seeds for each run.

For this scenario, we computed slopes for Lipschitz bounds starting from depth 2. The slopes for the upper, lower, and average Lipschitz bounds for *trained networks* are: 3.33, 2.03, 1.19 respectively and are computed by examining the slope coefficient of a linear regression model fitted to the corresponding values in the log-log scale. The  $R^2$  values of the fit for the upper, lower, and average Lipschitz bounds are: 0.9749, 0.9483 and 0.8798 respectively. For networks *at initialisation*, slopes from depth 2 for the upper, lower, and average Lipschitz bounds are 0.30, -2.52 and -2.84 respectively.

### S1.5.12 Effect of the number of training samples on the Lipschitz constant (Section 5.4)

For this experiment we trained 4 types of FCN ReLU 256 models on different sizes of MNIST1D: 4000, 1000, 500 and 100 training samples. Sampling was performed by taking a random subsample from the main dataset. Each model was trained with batch size 512 using Cross-Entropy loss and the SGD optimiser, 0.005 learning rate and Warmup20000Step25 LR scheduler (see S1.4). We trained our models for at least 10,000 epochs and stopped each model when either 0.01 gradient norm is reached or when 300,000 epochs have passed. We trained 4 seeds for each run.

### S1.5.13 Effect of shuffling labels for the train set on (Figure 8 and Section S2.8)

For this experiment, we trained 4 types of CNN models (CNN 7, CNN 10, CNN 20 and CNN 60) on a fixed subset of 5000 samples from CIFAR-10 with various amounts of shuffled labels ( $\alpha$  parameter): 0%, 10%, 20%, 30%, 40%, 50%, 60%, 70%, 80%, 90% and 100%. Each shuffle is incremental, meaning that all shuffles from a dataset with a smaller  $\alpha$  are contained in the dataset with a larger  $\alpha$ . CIFAR-10 subsets and shuffles are fixed among seeds. Each model was trained with batch size 128 using Cross-Entropy loss and the SGD optimiser, 0.05 learning rate and Cont100 LR scheduler (see S1.4). We trained our models for at least 1,000 epochs and stopped each model when either 0.01 gradient norm is reached or when 5,000 epochs have passed. We trained 4 seeds for each run.

*Comment on the minimum number of epochs.* In comparison to the similar Double Descent setup (see S1.5.3) we use a larger number of minimum epochs in this experiment, since smaller models require more updates to escape the initialisation well, especially in presence of label noise (see S1.3).

## S2 Additional experiments

### S2.1 Estimation of the potential error of evaluating lower Lipschitz bound by considering a subsample of ImageNet

Due to computational limitations, in the ResNet50 evolution experiment (see Section 4.2) we evaluate the lower Lipschitz bound on a subset of ImageNet. This decision would naturally produce a weaker estimate of the Lipschitz constant, compared to the full dataset evaluation, raising concerns on the representativeness of the lower bound in the first place. Therefore we conducted a small investigation into the magnitude of potential error due to ImageNet subsampling for the ResNet18 case.

In this analysis, we took the distribution of Jacobian norms for pretrained ResNet18, evaluated for the whole ImageNet training dataset (see S1.5.7 for more details), and estimated the lower bound for various random subsets of computed norms. Results are depicted in Table S3. According to the obtained statistics, doubling the subset size decreases the relative error by around 5%, suggesting that moderate errors can be achieved for rather small subsets. These results motivated our decision of using 200,000 as our subsample size — a plausible trade-off between computational burden and estimation accuracy.

Subset size	Estimate	St.dev.	Percentage difference to true estimate
50,000	220.50	23.72	20.87%
100,000	234.95	23.49	15.69%
200,000	249.28	21.24	10.54%
300,000	257.02	18.85	7.76%
400,000	262.15	16.86	5.92%

Table S3: Estimates of the lower bound for trained ResNet18 on the different subsets of ImageNet. Estimates are averaged over 1000 random subsets.

### S2.2 Lipschitz evolution for other settings

In this section, we present evolution plots for settings that were mentioned in Section 4.1. We start with evolution plots for FCN networks with MSE loss and then continue with CNN evolution on



CIFAR-10 and MNIST. Table S4 shows the values of the corresponding slopes with linear regression  $R^2$  metrics for each setup.

Evolution plot	Slopes	$R^2$ metric
FCN, MNIST1D, CE loss (Fig. 2)	0.59, <b>0.46</b> , 0.44	0.9955, <b>0.9986</b> , 0.9980
FCN, MNIST1D, MSE loss (Fig. S2)	0.80, <b>0.62</b> , 0.52	0.9982, <b>0.9914</b> , 0.9991
CNN, CIFAR-10, CE loss (Fig. S3)	0.22, <b>0.29</b> , 0.29	0.9461, <b>0.9327</b> , 0.9460
ResNet50, subset of ImageNet, CE loss (Fig. 3)	7.32, <b>0.49</b> , 0.48	0.8441, <b>0.9718</b> , 0.8774

Table S4: Estimates of the slopes and linear regression  $R^2$  metrics for the upper, **lower** and average norm Lipschitz bounds for various evolution plots.

From Table S4, one can clearly see how the slope for the upper bound is larger for some more complex models and datasets. Consequently, a simple upper bound is an excessively loose estimator of the Lipschitz constant — despite its theoretical full input domain coverage, this estimator has little practical value due to excessive overestimation. As discussed in detail in Section 4.1, we therefore suggest paying close attention to the lower bound estimator. It would intriguing to see how tighter upper bound estimates compare to our lower and upper bounds, but we leave this investigation for future work.

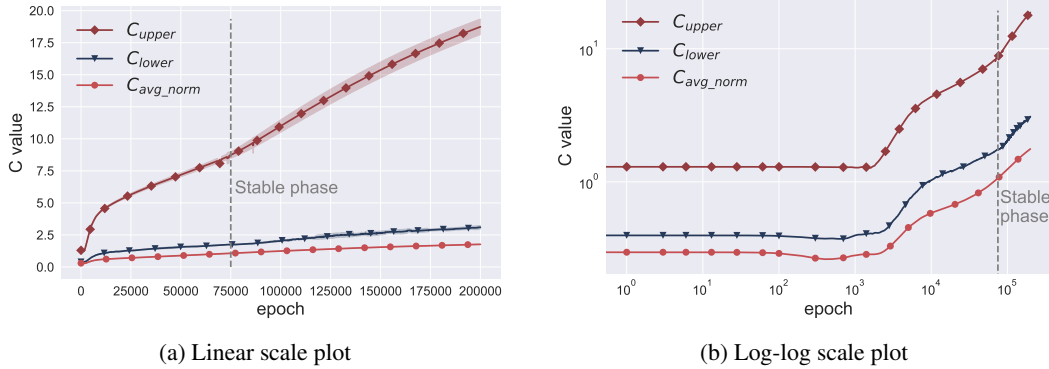
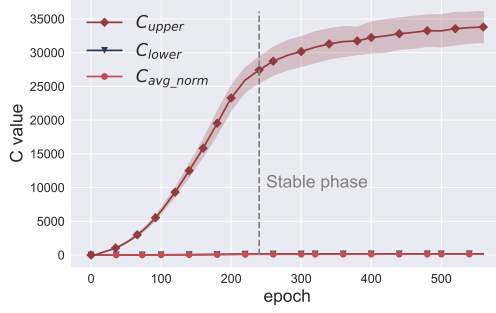
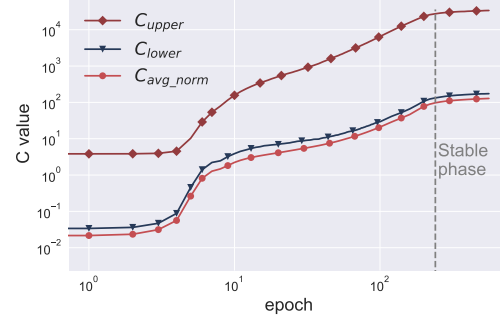


Figure S2: Lipschitz constant bounds evolution for **FCN ReLU 256**. The model was trained on **MNIST1D** using MSE loss and SGD optimiser. Results are averaged over 4 runs. Stable phase is considered to start after epoch 75,000. We took this model form the Double Descent experiment (see Appendix S1.5.2).

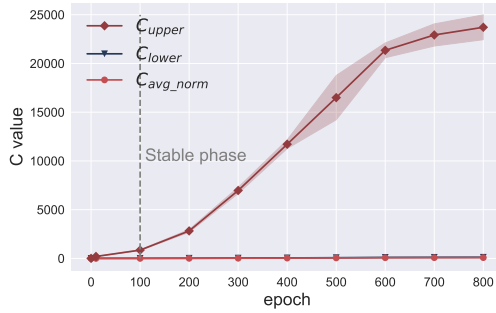


(a) Linear scale plot

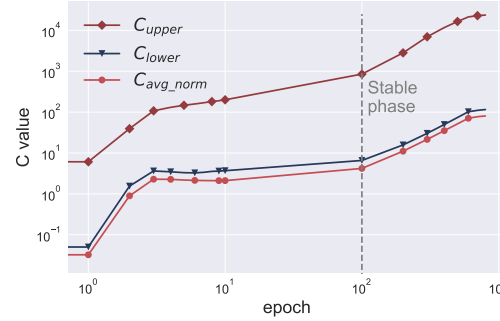


(b) Log-log scale plot

Figure S3: Lipschitz constant bounds evolution for **CNN 20**. The model was trained on **CIFAR-10** using Cross-Entropy loss and SGD optimiser. Results are averaged over 4 runs. Stable phase is considered to start after epoch 240. We used the same setup as in the Double Descent experiment (see Appendix S1.5.3).



(a) Linear scale plot



(b) Log-log scale plot

Figure S4: Lipschitz constant bounds evolution for **CNN 20**. The model was trained on **MNIST with 10% labels shuffled** using Cross-Entropy loss and SGD optimiser. Results are averaged over 4 runs. Stable phase is considered to start after epoch 100. We took this model form the Double Descent experiment (see Appendix S1.5.4).

### S2.3 Lipschitz Double Descent for other settings

This section showcases Lipschitz constant Double Descent plots for settings mentioned in Section 4.3.

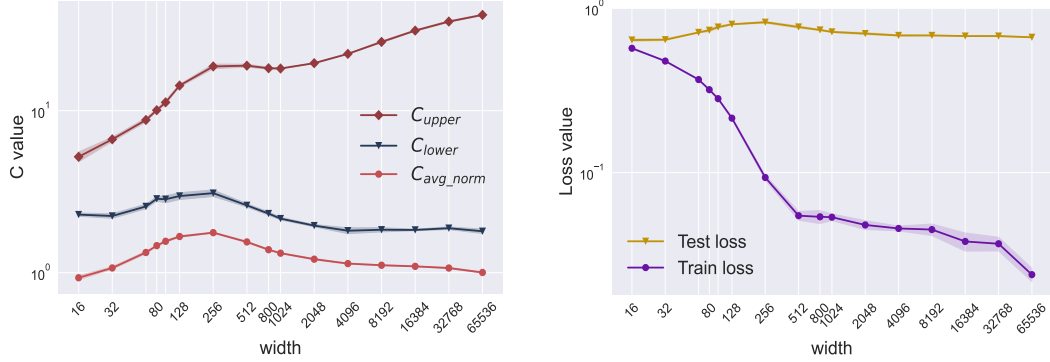


Figure S5: Comparison of various Lipschitz constant bounds with train and test losses with increasing hidden layer width, in the case of **FCN ReLU networks** on **MNIST1D** with **MSE loss**. Results are averaged over 4 runs. More details about the networks and the training strategy are listed in Appendix S1.5.2.

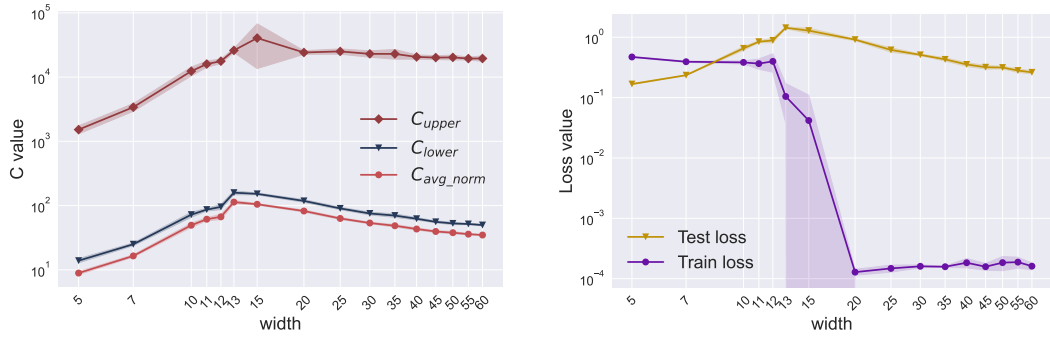


Figure S6: Comparison of various Lipschitz constant bounds with train and test losses with increasing hidden layer width, in the case of **CNN networks** on **MNIST with 10% of labels shuffled** with **Cross-Entropy loss**. Results are averaged over 4 runs. More details about the networks and the training strategy are listed in Appendix S1.5.4.

## S2.4 More experiments on the Lipschitz constant in the Double Descent setting

This section includes experiments, where we compute Lipschitz constant bounds for a set of models from another study [37]. Results are produced from training a series of fully connected networks on CIFAR-10 and MNIST with MSE loss. This solidifies our findings on Lipschitz’s Double Descent trends.

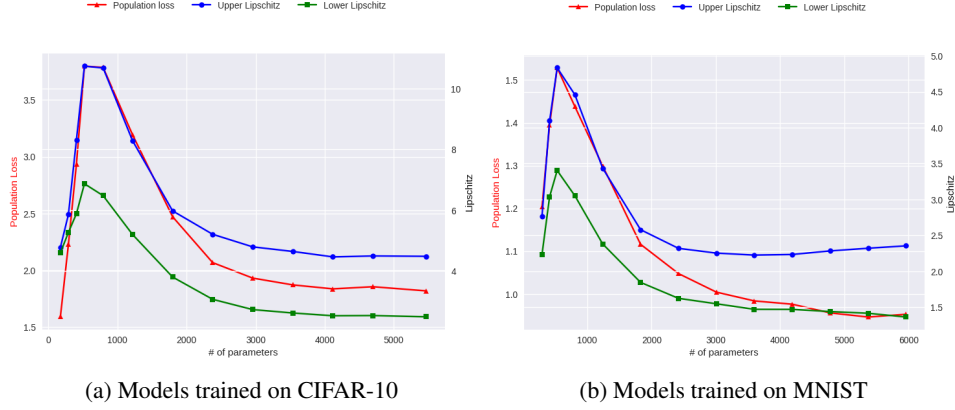


Figure S7: Plot of Lipschitz constant bounds for fully connected networks with 1 hidden layer, trained using SGD with MSE loss.

## S2.5 Bias-Variance trade-off evaluation

In Section 4.3, we showed the equation for the bias-variance trade-off for the expected test loss. We then proceeded with upper bounding the variance, ignoring the effect of bias. In Figure S8 we display the results of the empirical bias-variance decomposition of the test loss for the MNIST1D Double Descent scenario (see Appendix S1.5.2 for more details). The plot reveals that the Double Descent shape is mostly governed by the variance term, whereas the bias is almost constant across widths.

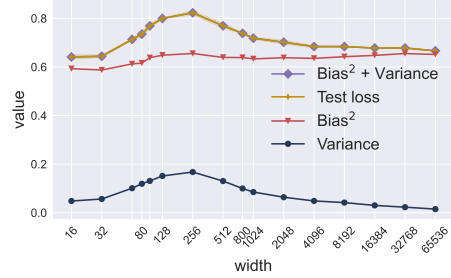


Figure S8: Bias-Variance decomposition of the expected test loss.

## S2.6 Optimising the upper bound for the Variance

As discussed in Section 4.3 (and more comprehensively in Appendix S3.2), the variance of the learned function is related to the Lipschitz constant by following equation:

$$\mathbb{E}_{\mathbf{x} \sim S'} \text{Var}_{\zeta}(f_{\theta}(\mathbf{x}, \zeta)) \leq 3(\overline{C}^2 + \overline{C}_{\zeta}^2) \mathbb{E}_{\mathbf{x} \sim S'} \|\mathbf{x}\|^2 + 3 \text{Var}_{\zeta}(f_{\theta}(\mathbf{0}, \zeta)) \quad (\text{Var bound 1})$$

According to Figure 7, variance bounds are rather loose compared to the variance itself. We contribute this difference to the large value of dataset radius  $\mathbb{E}_{\mathbf{x} \sim S'} \|\mathbf{x}\|^2$  which can potentially be optimised by choosing a better  $\mathbf{x}'$  in bound Var bound 0. For this case, the optimal minimum for  $\mathbb{E}_{\mathbf{x} \sim S'} \|\mathbf{x} - \mathbf{x}'\|^2$  is  $\mathbf{x}' = \mathbb{E}_{\mathbf{x} \sim S'}[\mathbf{x}] = \bar{\mathbf{x}}$ , which we utilised to recompute the bound in Figure S9.

In the case of MNIST1D, the bound is only almost negligibly better due to  $\bar{\mathbf{x}}$  being close to a zero vector for this particular dataset. We leave further analysis of improving the upper variance bound tightness for future work.

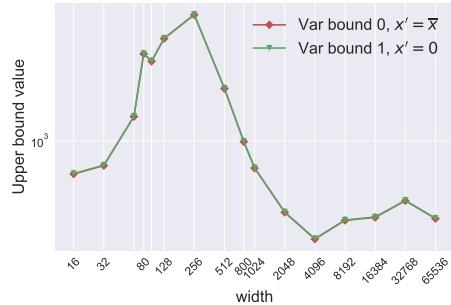


Figure S9: Optimised variance bound compared with Var bound 1 and variance.

## S2.7 Variance bounds for the complete sweep of widths

In this section we present the omitted plot of the evaluation of variance upper bounds for the whole sweep of widths for MNIST1D. Results are shown in Figure S10.

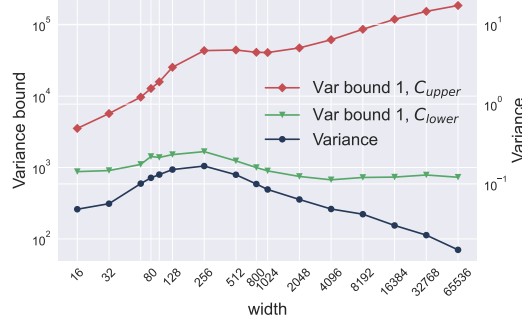


Figure S10: Variance and its upper bounds, where  $\overline{C_\zeta}$  in Var bound 1 is estimated using  $C_{\text{lower}}$  and  $C_{\text{upper}}$  estimates. Results are presented from training FCN LeakyReLU networks with varying width on MNIST1D using MSE loss. The expectations over random initialisations were computed as an average of 4 seeds. More details in Appendix S1.5.8.

## S2.8 More experiments on the effect of label noise

As mentioned in Section 4.4, we attributed the enigmatic decrease of the Lipschitz constant for over-parametrised networks to the small distance that the model has to travel from initialisation to find the solution. To further support our claims, we provide the results of evaluating the norm of the parameter distance (i.e.  $\text{param\_dist}_\tau = \sum_{t=1}^{\tau} \|\theta^t - \theta^{t-1}\|_2$ , where  $t$  iterates through saved model checkpoints) for CNN 7 and CNN 60 in a similar setting, as well as upper and average norm bounds for the whole sweep of networks.

*Remark.* In most figures, especially for CNN 60 (Fig. S14), parameter distance resembles the upper bound shape more closely than the lower bound. However, since the true Lipschitz constant still lies between the two bounds, the evidence still supports our hypothesis in Section 4.4.

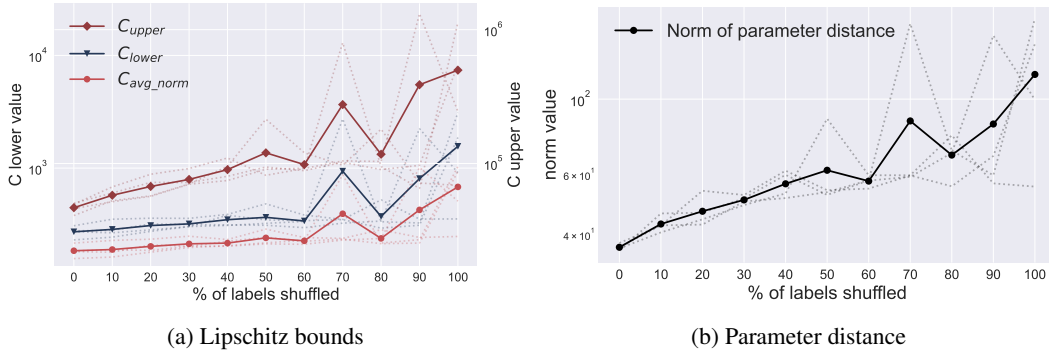
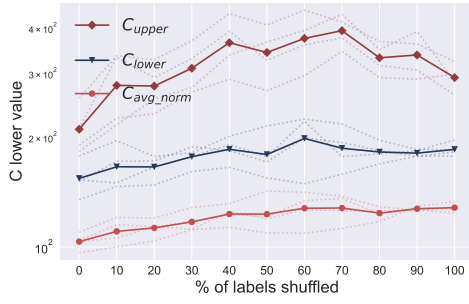
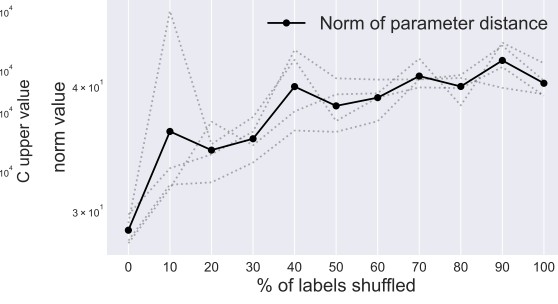


Figure S11: Summary of Lipschitz constant bounds for various levels of label shuffling for CNN 7 trained on a subset of CIFAR-10. More details in Appendix S1.5.13.



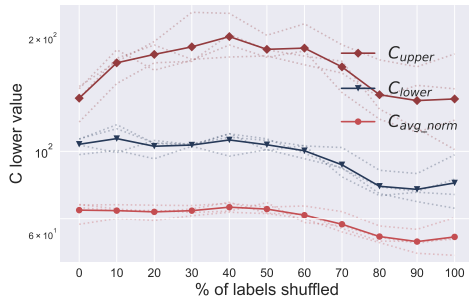


(a) Lipschitz bounds

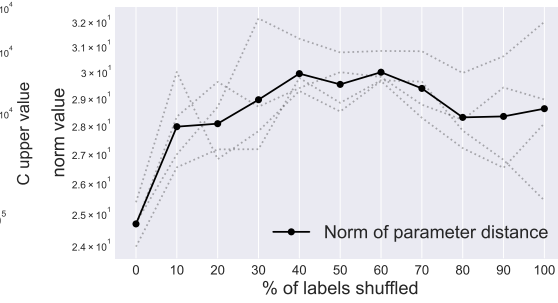


(b) Parameter distance

Figure S12: Summary of Lipschitz constant bounds for various levels of label shuffling for **CNN 10** trained on a subset of CIFAR-10. More details in Appendix S1.5.13.

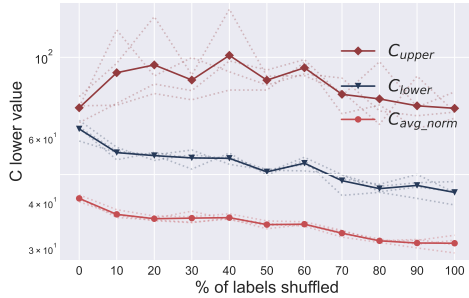


(a) Lipschitz bounds

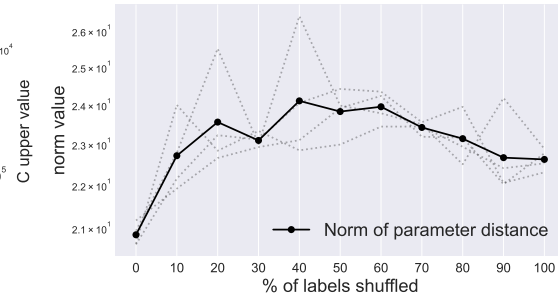


(b) Parameter distance

Figure S13: Summary of Lipschitz constant bounds for various levels of label shuffling for **CNN 20** trained on a subset of CIFAR-10. More details in Appendix S1.5.13.



(a) Lipschitz bounds



(b) Parameter distance

Figure S14: Summary of Lipschitz constant bounds for various levels of label shuffling for **CNN 60** trained on a subset of CIFAR-10. More details in Appendix S1.5.13.

## S2.9 ResNet50 upper bound on more checkpoints

Since computing the Lipschitz upper bound is significantly less expensive than the lower bound for the case of ResNet50 evolution, we have additionally evaluated the upper bound on a finer set of checkpoints for one seed to present a more complete picture of the upper bound evolution. According to the results in Figure S15, the upper bound slope after epoch 60 is 7.04 with  $R^2$  0.9624, supporting the representativeness of our previous estimation.

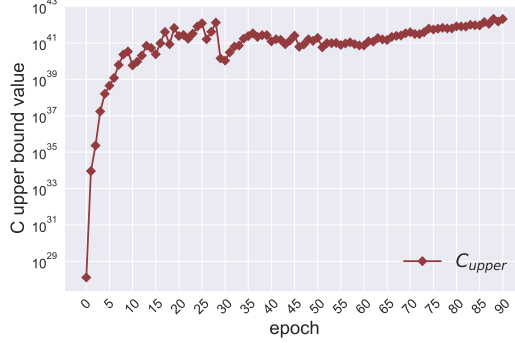


Figure S15: Upper Lipschitz constant bounds evolution for ResNet50. More details in Appendix S1.5.6.

## S2.10 Jacobian norm distributions for other models and datasets.

In Section 4.2 we have shown a distribution of the norm of the per-sample Jacobian for pretrained ResNet18. Here we provide additional plots for other types of models and datasets. In particular, we showcase the distribution plots for FCNs trained on MNIST1D with Cross-Entropy and MSE losses, CNNs trained on CIFAR-10 and MNIST with 10% label noise and, finally, ResNets on CIFAR-10 (we used pretrained models from [47]). All norms are evaluated on the datasets used for training. Each dotted line represents the maximum norm, or, in other words, the lower Lipschitz bound estimate.

In comparison to just the lower Lipschitz bound estimate, the Jacobian norm distribution plot provides more information on the continuity of the function in the training domain. If the distribution has a long right tail, like in the case of ResNets in Figure S20, the corresponding function has to be rather smooth in the vicinity of most samples, while being more vulnerable to drastic changes for a smaller subset of inputs. It would be fascinating to see if the skewness of this distribution bears a connection to the difficulty of generating adversarial examples, but we leave this direction for future research.

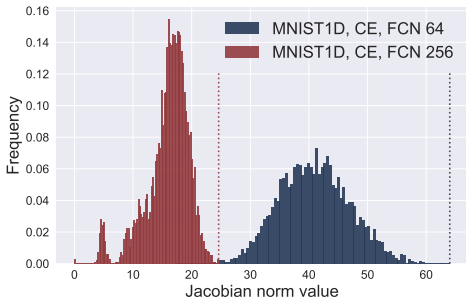


Figure S16: Distribution of the norm of the per-sample Jacobian for FCN ReLU 64 and FCN ReLU 256, trained on MNIST1D with **Cross-Entropy loss**. See Appendix S1.5.1 for training details.

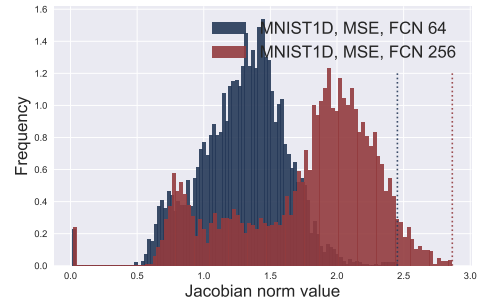


Figure S17: Distribution of the norm of the per-sample Jacobian for FCN ReLU 64 and FCN ReLU 256, trained on MNIST1D with **MSE loss**. See Appendix S1.5.2 for training details.

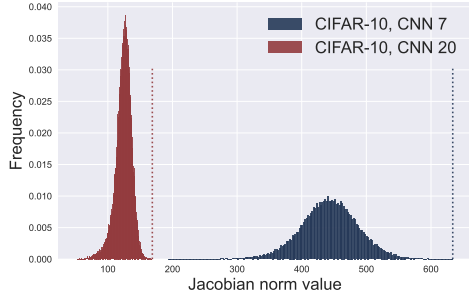


Figure S18: Distribution of the norm of the per-sample Jacobian for CNN 7 and CNN 20, trained on **CIFAR-10**. See Appendix S1.5.3 for training details.

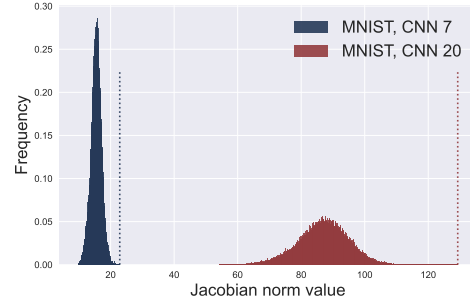


Figure S19: Distribution of the norm of the per-sample Jacobian for CNN 7 and CNN 20, trained on **MNIST with 10% label noise**. See Appendix S1.5.4 for training details.

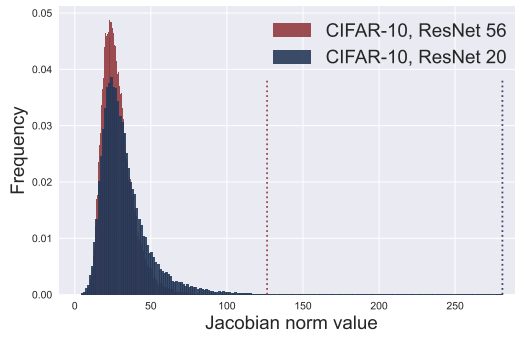


Figure S20: Distribution of the norm of the per-sample Jacobian for ResNet 20 and ResNet 56, trained on CIFAR-10. We refer to [47] for training details.

## S3 Theoretical proofs

### S3.1 Theoretical analysis of Lipschitz evolution

Let us denote  $f(\boldsymbol{\theta}, \mathbf{x}) : \mathbb{R}^p \times \mathbb{R}^d \mapsto \mathbb{R}^K$  as our network function, where  $\boldsymbol{\theta}$  is our parameter vector. We also denote  $\mathcal{L}(\boldsymbol{\theta}, S)$  as our loss and  $S$  as our training set. We are interested in finding a bound for  $C$  for the trained model at time step  $T$ :

$$\forall \mathbf{x}, \mathbf{x}' \in \mathcal{D} : \|f(\boldsymbol{\theta}^T, \mathbf{x}) - f(\boldsymbol{\theta}^T, \mathbf{x}')\| \leq C \|\mathbf{x} - \mathbf{x}'\| \leq C \underbrace{\sup_{\mathbf{x}, \mathbf{x}' \in \mathcal{D}} \|\mathbf{x} - \mathbf{x}'\|}_{=r}$$

**Initial and Final points based analysis.** Let us introduce a simple upper bound on the LHS by adding and subtracting the network at initialisation:

$$\begin{aligned} \|f(\boldsymbol{\theta}^T, \mathbf{x}) - f(\boldsymbol{\theta}^T, \mathbf{x}')\| &= \|f(\boldsymbol{\theta}^T, \mathbf{x}) - f(\boldsymbol{\theta}^0, \mathbf{x}) + f(\boldsymbol{\theta}^0, \mathbf{x}) - f(\boldsymbol{\theta}^0, \mathbf{x}') + f(\boldsymbol{\theta}^0, \mathbf{x}') - f(\boldsymbol{\theta}^T, \mathbf{x}')\| \\ &\leq \|f(\boldsymbol{\theta}^T, \mathbf{x}) - f(\boldsymbol{\theta}^0, \mathbf{x})\| + \|f(\boldsymbol{\theta}^0, \mathbf{x}) - f(\boldsymbol{\theta}^0, \mathbf{x}')\| + \|f(\boldsymbol{\theta}^0, \mathbf{x}') - f(\boldsymbol{\theta}^T, \mathbf{x}')\| \\ &\leq 2C_{\boldsymbol{\theta}}^{\text{global}} \|\boldsymbol{\theta}^0 - \boldsymbol{\theta}^T\| + C_{\mathbf{x}}(\boldsymbol{\theta}^0) \|\mathbf{x} - \mathbf{x}'\| \\ &\leq 2C_{\boldsymbol{\theta}}^{\text{global}} \|\boldsymbol{\theta}^0 - \boldsymbol{\theta}^T\| + C_{\mathbf{x}}(\boldsymbol{\theta}^0) r, \end{aligned}$$

where  $C_{\mathbf{x}}(\boldsymbol{\theta}^0)$  is the Lipschitz constant in the input space for the model at initialisation and  $C_{\boldsymbol{\theta}}^{\text{global}}$  is the Lipschitz constant for the network in the parameter space. The latter quantity is unfortunately hard to compute, since it requires to search through the space of both parameters and inputs to find the maximum norm (thus it is marked as global). Moreover, it might not be as tight.

**Intermediate-points based analysis.** We can tackle the above issue by applying the same trick iteratively to get a local Lipschitz constant in the parameter space:

$$\begin{aligned} \|f(\boldsymbol{\theta}^T, \mathbf{x}) - f(\boldsymbol{\theta}^T, \mathbf{x}')\| &= \|f(\boldsymbol{\theta}^T, \mathbf{x}) + \sum_{t=0}^{T-1} (f(\boldsymbol{\theta}^t, \mathbf{x}) - f(\boldsymbol{\theta}^t, \mathbf{x}) + f(\boldsymbol{\theta}^t, \mathbf{x}') - f(\boldsymbol{\theta}^t, \mathbf{x}')) - f(\boldsymbol{\theta}^T, \mathbf{x}')\| \\ &\leq \sum_{t=0}^{T-1} \|f(\boldsymbol{\theta}^{t+1}, \mathbf{x}) - f(\boldsymbol{\theta}^t, \mathbf{x})\| + \sum_{t=0}^{T-1} \|f(\boldsymbol{\theta}^t, \mathbf{x}') - f(\boldsymbol{\theta}^{t+1}, \mathbf{x}')\| + \|f(\boldsymbol{\theta}^0, \mathbf{x}) - f(\boldsymbol{\theta}^0, \mathbf{x}')\| \\ &\leq 2C_{\boldsymbol{\theta}}^{\text{local}} \sum_{t=0}^{T-1} \|\boldsymbol{\theta}^{t+1} - \boldsymbol{\theta}^t\| + C_{\mathbf{x}}(\boldsymbol{\theta}^0) \|\mathbf{x} - \mathbf{x}'\| \\ &\leq 2C_{\boldsymbol{\theta}}^{\text{local}} \sum_{t=0}^{T-1} \|\boldsymbol{\theta}^{t+1} - \boldsymbol{\theta}^t\| + C_{\mathbf{x}}(\boldsymbol{\theta}^0) r, \end{aligned}$$

where  $C_{\boldsymbol{\theta}}^{\text{local}} := \sup_{\boldsymbol{\theta} \in \{\boldsymbol{\theta}^0, \dots, \boldsymbol{\theta}^T\}} \sup_{\mathbf{x} \in \text{dom}(f)} \|\nabla_{\boldsymbol{\theta}} f(\boldsymbol{\theta}, \mathbf{x})\|$ , i.e., the supremum of the local parameter-wise Lipschitz constants. In comparison to  $C_{\boldsymbol{\theta}}^{\text{global}}$ ,  $C_{\boldsymbol{\theta}}^{\text{local}}$  is only evaluated at training checkpoints  $(\boldsymbol{\theta}^0, \dots, \boldsymbol{\theta}^T)$ , reducing the search space in the parameter dimension (thus it is marked as local). If we assume bounded gradients (i.e.  $\|\nabla_{\boldsymbol{\theta}} \mathcal{L}(\boldsymbol{\theta}, \mathbf{x})\| \leq B$ ), we know that  $C_{\boldsymbol{\theta}}^{\text{local}}$  is also bounded:

$$B \geq \|\nabla_{\boldsymbol{\theta}} \mathcal{L}(\boldsymbol{\theta}, \mathbf{x})\| = \|\nabla_f \mathcal{L}(\boldsymbol{\theta}, \mathbf{x}) \cdot \nabla_{\boldsymbol{\theta}} f(\boldsymbol{\theta}, \mathbf{x})\| \geq \sigma_{\min}(\nabla_f \mathcal{L}(\boldsymbol{\theta}, \mathbf{x})) \|\nabla_{\boldsymbol{\theta}} f(\boldsymbol{\theta}, \mathbf{x})\|,$$

where  $\sigma_{\min}(\cdot)$  denotes the smallest singular value.

We can further simplify the equation by considering the GD update rule:  $\boldsymbol{\theta}^{t+1} = \boldsymbol{\theta}^t - \eta_t \nabla_{\boldsymbol{\theta}^t} \mathcal{L}(\boldsymbol{\theta}^t, S)$  and keeping the bounded gradients  $B$  assumption. The term  $\eta_t$  denotes the learning rate at time step

$t$ . Let  $\eta$  be the maximum learning rate throughout the epochs. Then we have the following:

$$\begin{aligned}
\|f(\boldsymbol{\theta}^T, \mathbf{x}) - f(\boldsymbol{\theta}^T, \mathbf{x}')\| &\leq 2C_{\boldsymbol{\theta}}^{\text{local}} \sum_{t=0}^{T-1} \|\boldsymbol{\theta}^{t+1} - \boldsymbol{\theta}^t\| + C_{\mathbf{x}}(\boldsymbol{\theta}^0)r \\
&\leq 2C_{\boldsymbol{\theta}}^{\text{local}} \sum_{t=0}^{T-1} \eta_t \|\nabla_{\boldsymbol{\theta}^t} \mathcal{L}(\boldsymbol{\theta}^t, S)\| + C_{\mathbf{x}}(\boldsymbol{\theta}^0)r \leq 2C_{\boldsymbol{\theta}}^{\text{local}} \sum_{t=0}^{T-1} \eta B + C_{\mathbf{x}}(\boldsymbol{\theta}^0)r \\
&= \left( \frac{2}{r} C_{\boldsymbol{\theta}}^{\text{local}} B \eta T + C_{\mathbf{x}}(\boldsymbol{\theta}^0) \right) r
\end{aligned}$$

Therefore the Lipschitz constant grows in proportion to the number of steps:

$$C \propto \left( \frac{2}{r} C_{\boldsymbol{\theta}}^{\text{local}} B \eta \right) T$$

### S3.2 Bias-Variance tradeoff

Let us denote the neural network function as  $f_{\boldsymbol{\theta}}(\mathbf{x}, S, \zeta)$  and the ground-truth function as  $\mathbf{y}^*(\mathbf{x})$ . Here,  $S$  denotes the training set and  $\zeta$  indicates the noise in the function due to the choice of random initialisation and the noise introduced by a stochastic optimiser, like stochastic gradient descent (SGD). In other words, one can take  $\zeta$  as denoting the random seed used in practice. Then let us assume we have the square loss, i.e.,  $\ell(\mathbf{x}; f_{\boldsymbol{\theta}}) = \|y(\mathbf{x}) - f_{\boldsymbol{\theta}}(\mathbf{x}, S, \zeta)\|^2$ . We can write the loss evaluated on a test set,  $S'$ , i.e., the test loss, as follows:

$$\mathcal{L}(\boldsymbol{\theta}, S', \zeta) = \mathbb{E}_{\mathbf{x} \sim S'} [\|y(\mathbf{x}) - f_{\boldsymbol{\theta}}(\mathbf{x}, S, \zeta)\|^2] \quad (7)$$

In practice, we typically average the test loss over several random seeds, hence inherently involving an expectation over the noise  $\zeta$ . We derive a bias-variance tradeoff [1, 48] that rests upon this as the noise source. Also, we consider the fixed-design variant of the bias-variance tradeoff and as a result, we will not average over the choice of the training set sampled from the distribution. In any case, for a suitably large training set size, this is expected not to introduce a lot of fluctuations and in particular, for the phenomenon at hand, i.e. Double Descent, the training set is generally considered to be fixed. Hereafter, for convenience, we will suppress the dependence of the network function on the training set.

Now we do the usual trick of adding and subtracting the expected neural network function over the noise source. Hence, we can rewrite the above as:

$$\begin{aligned}
\mathcal{L}(\boldsymbol{\theta}, S', \zeta) &= \mathbb{E}_{\mathbf{x} \sim S'} [\|y(\mathbf{x}) - \mathbb{E}_{\zeta}[f_{\boldsymbol{\theta}}(\mathbf{x}, \zeta)] + \mathbb{E}_{\zeta}[f_{\boldsymbol{\theta}}(\mathbf{x}, \zeta)] - f_{\boldsymbol{\theta}}(\mathbf{x}, \zeta)\|^2] \\
&= \mathbb{E}_{\mathbf{x} \sim S'} [\|y(\mathbf{x}) - \mathbb{E}_{\zeta}[f_{\boldsymbol{\theta}}(\mathbf{x}, \zeta)]\|^2] + \mathbb{E}_{\mathbf{x} \sim S'} [\|\mathbb{E}_{\zeta}[f_{\boldsymbol{\theta}}(\mathbf{x}, \zeta)] - f_{\boldsymbol{\theta}}(\mathbf{x}, \zeta)\|^2] \\
&\quad + 2 \mathbb{E}_{\mathbf{x} \sim S'} \left[ (y(\mathbf{x}) - \mathbb{E}_{\zeta}[f_{\boldsymbol{\theta}}(\mathbf{x}, \zeta)])^\top (\mathbb{E}_{\zeta}[f_{\boldsymbol{\theta}}(\mathbf{x}, \zeta)] - f_{\boldsymbol{\theta}}(\mathbf{x}, \zeta)) \right]
\end{aligned}$$

Next, we take the expectation of the above test loss with respect to the noise source  $\zeta$  — mirroring the empirical practice of reporting results averaged over multiple seeds. It is easy to see that when taking the expectation, the cross-term vanishes and we are left with the following expression:

$$\mathbb{E}_{\zeta} \mathcal{L}(\boldsymbol{\theta}, S', \zeta) = \mathbb{E}_{\mathbf{x} \sim S'} [\|y(\mathbf{x}) - \mathbb{E}_{\zeta}[f_{\boldsymbol{\theta}}(\mathbf{x}, \zeta)]\|^2] + \mathbb{E}_{\zeta} \mathbb{E}_{\mathbf{x} \sim S'} [\|\mathbb{E}_{\zeta}[f_{\boldsymbol{\theta}}(\mathbf{x}, \zeta)] - f_{\boldsymbol{\theta}}(\mathbf{x}, \zeta)\|^2] \quad (8)$$

$$= \mathbb{E}_{\mathbf{x} \sim S'} [\|y(\mathbf{x}) - \mathbb{E}_{\zeta}[f_{\boldsymbol{\theta}}(\mathbf{x}, \zeta)]\|^2] + \mathbb{E}_{\mathbf{x} \sim S'} \mathbb{E}_{\zeta} [\|\mathbb{E}_{\zeta}[f_{\boldsymbol{\theta}}(\mathbf{x}, \zeta)] - f_{\boldsymbol{\theta}}(\mathbf{x}, \zeta)\|^2] \quad (9)$$

$$= \mathbb{E}_{\mathbf{x} \sim S'} [\|y(\mathbf{x}) - \mathbb{E}_{\zeta}[f_{\boldsymbol{\theta}}(\mathbf{x}, \zeta)]\|^2] + \mathbb{E}_{\mathbf{x} \sim S'} \text{Var}_{\zeta}(f_{\boldsymbol{\theta}}(\mathbf{x}, \zeta)) \quad (10)$$

Overall, this results in the bias-variance trade-off under our setting.

**Upper-bounding the Variance term.** Now, we want to do a finer analysis of the variance term by involving the Lipschitz constant of the network function.

$$\text{Var}_\zeta(f_\theta(\mathbf{x}, \zeta)) = \mathbb{E}_\zeta [\|\mathbb{E}_\zeta[f_\theta(\mathbf{x}, \zeta)] - f_\theta(\mathbf{x}, \zeta)\|^2] \quad (11)$$

$$= \mathbb{E}_\zeta \left[ \left\| \underbrace{\mathbb{E}_\zeta[f_\theta(\mathbf{x}, \zeta)] - \mathbb{E}_\zeta[f_\theta(\mathbf{x}', \zeta)]}_a + \underbrace{\mathbb{E}_\zeta[f_\theta(\mathbf{x}', \zeta)] - f_\theta(\mathbf{x}', \zeta)}_b + \underbrace{f_\theta(\mathbf{x}', \zeta) - f_\theta(\mathbf{x}, \zeta)}_c \right\|^2 \right] \quad (12)$$

where, we have considered some auxiliary point  $\mathbf{x}'$ , and added and subtracted some terms. For  $n$  vectors,  $\mathbf{x}_1, \dots, \mathbf{x}_n$ , we can utilize the simple inequality:

$$\|\mathbf{x}_1 + \dots + \mathbf{x}_n\|^2 \leq n \sum_{i=1}^n \|\mathbf{x}_i\|^2$$

which follows from  $n$  applications of the Cauchy-Schwarz inequality. Hence, the variance above can be upper-bounded as:

$$\begin{aligned} \text{Var}_\zeta(f_\theta(\mathbf{x}, \zeta)) &\leq 3 \|\mathbb{E}_\zeta[f_\theta(\mathbf{x}, \zeta)] - \mathbb{E}_\zeta[f_\theta(\mathbf{x}', \zeta)]\|^2 + 3 \mathbb{E}_\zeta \|\mathbb{E}_\zeta[f_\theta(\mathbf{x}', \zeta)] - f_\theta(\mathbf{x}', \zeta)\|^2 \\ &\quad + 3 \mathbb{E}_\zeta \|f_\theta(\mathbf{x}', \zeta) - f_\theta(\mathbf{x}, \zeta)\|^2 \end{aligned}$$

We can think of  $\mathbb{E}_\zeta f_\theta(\mathbf{x}, \zeta)$  as the ensembled function mapping, and denote it by saying  $\overline{f}_\theta(\mathbf{x}) := \mathbb{E}_\zeta f_\theta(\mathbf{x}, \zeta)$ , and let's assume that it is  $\overline{C}$ -Lipschitz. On the other hand, let's say that each individual function  $f_\theta(\mathbf{x}, \zeta)$  has Lipschitz constant  $C_\zeta$ . Hence we can further reduce the upper bound to

$$\text{Var}_\zeta(f_\theta(\mathbf{x}, \zeta)) \leq 3 \overline{C}^2 \|\mathbf{x} - \mathbf{x}'\|^2 + 3 \text{Var}_\zeta(f_\theta(\mathbf{x}', \zeta)) + 3 \mathbb{E}_\zeta C_\zeta^2 \|\mathbf{x} - \mathbf{x}'\|^2. \quad (13)$$

Now, we bring back the outer expectation with respect to samples from the test set, i.e.,  $\mathbf{x} \sim S'$ :

$$\mathbb{E}_{\mathbf{x} \sim S'} \text{Var}_\zeta(f_\theta(\mathbf{x}, \zeta)) \leq 3 \mathbb{E}_{\mathbf{x} \sim S'} \overline{C}^2 \|\mathbf{x} - \mathbf{x}'\|^2 + 3 \mathbb{E}_{\mathbf{x} \sim S'} \text{Var}_\zeta(f_\theta(\mathbf{x}', \zeta)) + 3 \mathbb{E}_{\mathbf{x} \sim S'} \mathbb{E}_\zeta C_\zeta^2 \|\mathbf{x} - \mathbf{x}'\|^2$$

Notice that while the Lipschitz constant of the neural network function do depend on the training data, the above expectation is with respect to samples from the test set. Hence, we can take the Lipschitz constants that appear above outside of the expectation. Besides, the middle term on the right-hand side has no dependency on the test sample  $\mathbf{x} \sim S'$  and so the expectation goes away. Overall, this yields,

$$\mathbb{E}_{\mathbf{x} \sim S'} \text{Var}_\zeta(f_\theta(\mathbf{x}, \zeta)) \leq 3 (\overline{C}^2 + \overline{C}_\zeta^2) \mathbb{E}_{\mathbf{x} \sim S'} \|\mathbf{x} - \mathbf{x}'\|^2 + 3 \text{Var}_\zeta(f_\theta(\mathbf{x}', \zeta)) \quad (\text{Var bound 0})$$

where, for simplicity, we have denoted the Lipschitz constant  $C_\zeta$  averaged over the random seeds  $\zeta$ , as  $\overline{C}_\zeta$ . We can simplify the above upper bounds by taking  $\mathbf{x}' = \mathbf{0}$  as the vector of all zeros, resulting in:

$$\mathbb{E}_{\mathbf{x} \sim S'} \text{Var}_\zeta(f_\theta(\mathbf{x}, \zeta)) \leq 3 (\overline{C}^2 + \overline{C}_\zeta^2) \mathbb{E}_{\mathbf{x} \sim S'} \|\mathbf{x}\|^2 + 3 \text{Var}_\zeta(f_\theta(\mathbf{0}, \zeta)) \quad (\text{Var bound 1})$$